

Niemeyer, M., et al

Running head:

Degron flexibility enforces auxin sensing

Keywords: intrinsic disorder, degron, auxin, AUX/IAA, SCF^{TIR1}, phytohormones, allostery

Corresponding Author:

Luz Irina A. Calderón Villalobos

Molecular Signal Processing Department

Leibniz Institute of Plant Biochemistry (IPB)

Weinberg 3, D-06120 Halle (Saale)

Germany

Email: LuzIrina.Calderon@ipb-halle.de

Tel. +49 345 5582 1232

Fax. +49 345 5582 1209

Niemeyer, M., et al

Flexibility of intrinsically disordered degrons in AUX/IAA proteins reinforces auxin co-receptor assemblies

Michael Niemeyer¹, Elena Moreno Castillo¹, Christian H. Ihling², Claudio Iacobucci², Verona Wilde¹, Antje Hellmuth¹, Wolfgang Hoehenwarter³, Sophia L. Samodelov^{4,6}, Matias D. Zurbriggen⁴, Panagiotis L. Kastritis^{5,7,8}, Andrea Sinz², Luz Irina A. Calderón Villalobos^{1*}

¹*Department of Molecular Signal Processing, Leibniz Institute of Plant Biochemistry (IPB), Weinberg 3, D-06120 Halle (Saale), Germany;* ²*Department of Pharmaceutical Chemistry & Bioanalytics, Institute of Pharmacy, Martin-Luther University Halle-Wittenberg, Charles Tanford Protein Center, Kurt-Mothes-Str. 3a, D-06120 Halle (Saale) , Germany;* ³*Proteome Analytics Research Group Leibniz Institute of Plant Biochemistry (IPB), Weinberg 3, D-06120 Halle (Saale), Germany;* ⁴*Institute of Synthetic Biology & Cluster of Excellence on Plant Science (CEPLAS), Heinrich-Heine University of Düsseldorf, Universitätsstrasse 1, D-40225 Düsseldorf, Germany;* ⁵*Interdisciplinary Research Center HALOmem, Charles Tanford Protein Center, Martin Luther University Halle-Wittenberg, Kurt-Mothes-Straße 3a, D-06120 Halle (Saale), Germany;* ⁶*UniversitätsSpital Zürich, Rämistrasse 100, CH-8091 Zürich, Switzerland;* ⁷*Institute of Biochemistry and Biotechnology, Martin-Luther University Halle-Wittenberg, Kurt-Mothes-Straße 3, D-06120 Halle (Saale), Germany;* ⁸*Biozentrum, Martin Luther University Halle-Wittenberg, Weinbergweg 22, Halle/Saale, Germany*

*Corresponding author. Email: LuzIrina.Calderon@ipb-halle.de

Niemeyer, M., et al

1 **ABSTRACT (139 words)**

2 Cullin RING-type E3 ubiquitin ligases SCF^{TIR1/AFB1-5} and their ubiquitylation targets,
3 AUX/IAAs, sense auxin concentrations in the nucleus. TIR1 binds a surface-
4 exposed degron in AUX/IAAs promoting their ubiquitylation and rapid auxin-
5 regulated proteasomal degradation. Here, we resolved TIR1·auxin-IAA7 and
6 TIR1·auxin-IAA12 complex topology, and show that flexible intrinsically disordered
7 regions (IDRs) in the degron's vicinity, cooperatively position AUX/IAAs on TIR1. The
8 AUX/IAA PB1 interaction domain also assists in non-native contacts, affecting
9 AUX/IAA dynamic interaction states. Our results establish a role for IDRs in
10 modulating auxin receptor assemblies. By securing AUX/IAAs on two opposite
11 surfaces of TIR1, IDR diversity supports locally tailored positioning for targeted
12 ubiquitylation, and might provide conformational flexibility for adopting a multiplicity
13 of functional states. We postulate IDRs in distinct members of the AUX/IAA family to
14 be an adaptive signature for protein interaction and initiation region for proteasome
15 recruitment.

Niemeyer, M., et al

16 **Main text**

17 Proteolysis entails tight spatiotemporal regulation of cellular protein pools ^{1,2}. The
18 ubiquitin-proteasome system (UPS) rules over protein turnover, and controls
19 stimulation or attenuation of gene regulatory networks, depending on whether a
20 degradation target is a transcriptional repressor or activator ². A typical E1-E2-E3
21 enzymatic cascade warrants specific target ubiquitylation by catalyzing the ATP-
22 dependent attachment of ubiquitin moieties to the target ³. Directly and indirectly, every
23 single aspect of cellular integrity and adaptation is impacted by target ubiquitylation,
24 e.g. cell cycle progression, apoptosis/survival, oxidative stress, differentiation and
25 senescence ⁴. In SKP1/CULLIN1/F-BOX PROTEIN (SCF)-type E3 ubiquitin ligases,
26 the interchangeable F-BOX PROTEIN (FBP) determines specificity to the E3 through
27 direct physical interactions with the degradation target ^{5,6}. UPS targets carry a short
28 degradation signal or degron, located mostly within structurally disordered regions,
29 which is precisely recognized by cognate E3 ligases ⁷. Structural disorder and
30 conformational flexibility within UPS targets confer diversity and specificity on
31 regulated protein ubiquitylation and degradation ⁷. Primary degrons within a protein
32 family, whose members share the same fate, behave as islands of sequence
33 conservation surrounded by fast divergent intrinsically disordered regions (IDRs) ⁷.
34 Once a favorable E3-target association stage has been accomplished, one or multiple
35 lysines residues neighboring IDRs of the target, often form a ubiquitylation zone of
36 functional exposed ubiquitylation sites ⁸⁻¹⁰. Local disorder and conformational flexibility
37 brings next an E2-loaded with Ub (E2~Ub) into close proximity to the bound target,
38 such that a suitable microenvironment for catalytic Ub transfer is created ⁷. Efficient
39 degradation of UPS targets requires the 26S proteasome to bind its protein target
40 through a polyubiquitin chain with a specific topology, and subsequently engages the

Niemeyer, M., et al

41 protein at a flexible initiation region for unfolding and degradation ¹¹. A primary degron
42 for E3 recruitment, a ubiquitin chain, and an IDR in UPS targets build a tripartite
43 degron, required for efficient proteasome-mediated degradation ⁷.

44 Intrinsically disordered proteins (IDPs) often function in processes that underlie
45 phenotypic plasticity such as signal transduction in plants ¹²⁻¹⁵. Auxin promotes plant
46 growth and development by triggering an intracellular signaling cascade that leads to
47 changes in gene expression ¹⁶. INDOLE-3-ACETIC ACID proteins (AUX/IAAs) are
48 mostly short-lived transcriptional repressors, with half-lives varying from ~6-80 min,
49 and whose expression is largely and very rapidly (less than 15 minutes) stimulated by
50 auxin ¹⁷. The *Arabidopsis* genome encodes for 29 AUX/IAAs, with 23 of them carrying
51 a mostly conserved V_GWPP-[VI]-[RG]-x(2)-R degron as recognition signal for an
52 SCF^{TIR1/AFB1-5} E3 ubiquitin ligase for auxin-mediated AUX/IAA ubiquitylation and
53 degradation ^{18,19}. Under low auxin concentrations, AUX/IAAs repress type A AUXIN
54 RESPONSE FACTORS (ARF) transcription factors via physical heterotypic
55 interactions through their type I/II Phox/Bem1p (PB1) domain ¹⁹. Once specific cells
56 reach an intracellular auxin concentration threshold, F-BOX PROTEINS TRANSPORT
57 INHIBITOR RESPONSE 1 (TIR1)/AUXIN SIGNALING F-BOX 1-5 (AFB1-5) increase
58 their affinity for the AUX/IAA degron ^{20,21}. This results in an AUX/IAA ubiquitylation and
59 degradation cycle that enables derepression of the transcriptional machinery ²². Since
60 AUX/IAAs are themselves auxin regulated, once the intracellular AUX/IAA pool is
61 replenished, they act again in a negative feedback loop repressing ARF activity ^{23,24}.

62 Degron-carrying AUX/IAAs and TIR1/AFB1-5 form an auxin receptor system, as auxin
63 occupies a binding pocket in TIR1 just underneath the AUX/IAA degron ²⁰. Auxin
64 binding properties of the receptor complex are greatly determined by the specific
65 AUX/IAA engaged in the receptor complex ²¹. Hence, different combinations of

Niemeyer, M., et al

66 TIR1/AFBs and AUX/IAAs assemble at different auxin concentrations, allowing the
67 sensing of fluctuating intracellular auxin concentrations ²¹.

68 Although we currently lack structural information on AUX/IAAs, they are postulated to
69 adopt a modular structure according to sequence homology in different plant species
70 e.g. 29, 3, 1 members in *Arabidopsis thaliana*, *Physcomitrella patens*, and *Marchantia*
71 *polymorpha*, respectively ^{25,26}. Besides the primary degron motif, AUX/IAAs
72 encompass a TOPLESS interacting motif for transcriptional repression, and the PB1
73 C-terminal domain (CTD) ²⁷.

74 While the degron is absolutely necessary for AUX/IAA recruitment and degradation, it
75 is not sufficient for full auxin binding properties of a TIR1·AUX/IAA auxin receptor pair
76 ²¹. Intriguingly, unresolved flexible regions outside the primary degron contribute to
77 differential co-receptor assembly ²¹, AUX/IAA destabilization ^{28,29}, basal protein
78 accumulation ³⁰, and are also decorated with specific lysine residues that undergo
79 ubiquitylation *in vitro* ³¹.

80 The dynamic range of auxin sensitivity in plant cells, and by default growth and
81 developmental responses, relies on efficient AUX/IAA processing by the UPS that we
82 still need to mechanistically understand. The complexity of auxin signaling also
83 underscores the importance of unveiling precisely how different AUX/IAAs can
84 contribute to auxin sensing, engage in multifarious interactions, e.g. TIR1·AUX/IAA,
85 AUX/IAA·AUX/IAA and AUX/IAA·ARF, and undergo ubiquitylation and degradation.
86 While we recognize the degron as TIR1·AUX/IAA interaction motif, we lack information
87 on how AUX/IAAs are positioned on TIR1, or whether additional structural AUX/IAA
88 features might impact recruitment and auxin binding. Furthermore, full structure of

Niemeyer, M., et al

89 AUX/IAA proteins has remained elusive so far, as they appear to adopt a highly flexible
90 fold and/or form high order oligomers due to their PB1 domain.

91 Here, we studied the structural properties of AUX/IAAs and report on intrinsically
92 disordered regions (IDRs) in IAA7 and IAA12 that influence TIR1·AUX/IAA
93 interactions. We pursued a biochemical and structural proteomics approach and
94 unveiled how flexibility in AUX/IAAs affect their conformational ensemble allowing
95 surface accessibility of degrons. Our data demonstrate how an extended fold in
96 AUX/IAAs is favorable for recruitment by the SCF^{TIR1}, and offers a structural constraint
97 for correct positioning on TIR1. Our data lays evidence of how AUXIAAs are fully
98 recognized by the ubiquitylation machinery. We also offer a model of how a potential
99 allosteric effect that fine-tunes TIR1·AUX/IAA interactions echoes into AUX/IAA-
100 mediated control of gene expression.

101

102

Niemeyer, M., et al

103 Results

104 AUX/IAAs exhibit intrinsic structural disorder

105 Regions flanking the core GWPPVR degron motif influence AUX/IAA protein
106 recruitment by SCF^{TIR1}, impact auxin binding, and AUX/IAA degradation. A broader
107 sequence context of the AUX/IAA degron might be therefore crucial for the adequate
108 regulation of AUX/IAA processing and turnover, including post-translational
109 modifications (e.g. ubiquitylation), protein-protein interactions and ligand-protein
110 interactions^{21,28,29}. To probe whether structural flexibility and intrinsic disorder are
111 common features of AUX/IAAs in general, we carried out an *in silico* analysis
112 (IUPred2A) of the 29 members of the *Arabidopsis thaliana* AUX/IAA family (**Fig. 1a**,
113 **Supplementary Figs. 1**). This allows to predict global structural disorder along
114 AUX/IAA protein sequences, and to score the probability of disorder for every amino
115 acid residue in a context-dependent manner³². We also inspected the distribution of
116 IDRs in AUX/IAAs outside the well-structured PB1 domain (**Fig. 1a, Supplementary**
117 **Fig. 1**). We defined scores for disorder probability as high (= disordered, >0.6),
118 intermediate (0.4-0.6), or low (= ordered, <0.4). First, IDRs occur in most AUX/IAAs
119 and in almost all AUX/IAA subclades (**Fig. 1a**). IDR-located residues are enriched in
120 the N-terminal halves of AUX/IAAs and much less so in the C-terminal PB1-domains
121 (**Fig. 1a, Supplementary Fig. 1**). The length of the AUX/IAAs does not correlate with
122 an enrichment of disorder segments because IAA1-4 or IAA28 (average length below
123 200 aa) exhibit features of disorder, while similarly small AUX/IAAs (e.g. IAA6, IAA15,
124 IAA19, IAA32, or IAA34) are predicted to be well-structured. Interestingly, all non-
125 canonical AUX/IAAs but IAA33, which lacks the core degron motif for interaction with
126 TIR1 and auxin binding, are rather ordered. IAA33 diverged early during the evolution
127 from the rest of the AUX/IAAs³³, and it belongs, together with canonical IAA26 and

Niemeyer, M., et al

128 IAA13, to the most disordered family members. Intriguingly, AUX/IAAs such as IAA7
129 and IAA12, which are members of a different subclade ¹⁹, appear to have similar bias
130 for IDRs (**Fig. 1a, Supplementary Fig. 1**).

131 IAA7 and IAA12 equip TIR1·AUX/IAA receptor complexes with distinct auxin binding
132 affinities, *i.e.* K_d TIR1·IAA7 ~10 nM and TIR1·IAA12 ~ 300 nM, respectively ²¹. These
133 differences are not exclusive to a divergent primary degron, since a TIR1-IAA12^{GWPPVR}
134 co-receptor could not account for high auxin binding affinity ²¹. This data substantiated
135 the hypothesis that distinct features outside the core degron, such as IDRs, might
136 bestow AUX/IAAs, explicitly IAA7 and IAA12, with unique properties for interaction
137 with TIR1, and therefore auxin sensitivities. In order to investigate the distribution of
138 disorder in IAA7 and IAA12 proteins, we performed *in silico* analyses using multiple
139 disorder prediction algorithms (**Fig. 1b**). Consistently, all tested algorithms showed
140 that most of the disorder segments in IAA7 and IAA12 are located on their N-terminal
141 half (upstream of the PB1), and near their C-terminus resembling probably a
142 disordered “piggy tail”. We also observed an enrichment of hydrophilic residues in
143 these IDRs (hydropathy index), which may therefore be solvent exposed (**Fig. 1b**).
144 Disorder in IAA7 and IAA12 represents almost 50% of their amino acid content. In
145 IAA7 but most notably in IAA12, we observed a predominant “order-dip” corresponding
146 to the core degron (**Fig. 1b**).

147 Using recombinantly expressed proteins, we further analyzed IAA7 and IAA12
148 secondary structure and overall shape via CD spectroscopy and size exclusion
149 chromatography, respectively (**Fig. 1c-d, Supplementary Figs. 2-3**). Hereby, we
150 addressed a function-related transient AUX/IAA fold while considering different protein
151 conformational classes. In addition to wild-type and oligomerization-deficient IAA7 and
152 IAA12 full-length proteins (iaa7bm3, iaa12bm3), we incorporated truncated variants of

Niemeyer, M., et al

153 IAA7 and IAA12 lacking the compact PB1 domain. Both *iaa7bm3* and *iaa12bm3*
154 exhibit a rather complex mix of secondary structure elements characteristic of molten
155 globule-like proteins, displaying a minimum at ~205 nm, and a shoulder near 220 nm
156 in CD spectra ³⁴. CD spectra of PB1-lacking IAA7 and IAA12 appear to be shifted
157 toward a shorter wavelength with a minimum at just below 200 nm, which is
158 characteristic for random-coil proteins (**Fig. 1c, Supplementary Fig. 2**). **Figure 1d**
159 shows the measured Stokes radii (R_s) for *iaa7bm3*, *iaa12bm3* together with the
160 theoretical values of IAA7 and IAA12 displaying specific folds, v.z. native fold (NF),
161 molten globular (MG), premolten globule (PMG), and unfolded (IDP). Since, all
162 measured Stokes radii are larger than the ones expected for their respective natively
163 folded proteins, we concluded that *iaa7bm3* and *iaa12bm3* adapt extended structures
164 mainly due to large proportions of intrinsically disordered segments outside of the
165 compactly-folded PB1 domain.

166

167 **What is the impact of intrinsic disordered segments on auxin-dependent**
168 **SCF^{TIR1}-AUX/IAA associations?**

169 IAA7 and IAA12 as well as their sister proteins IAA14 and IAA13, respectively, exhibit
170 striking differences in their degron tail (**Supplementary Fig. 4**). While IAA7 and IAA14
171 have a short basic degron tail (<30 aa) linking the degron to the PB1 oligomerization
172 domain, IAA12 and IAA13 have a longer (44 aa), highly charged (Lys, Glu, Asp) and
173 unstructured degron tail (**Supplementary Fig. 4**). Because IAA7 and IAA12 have
174 distinct and contrasting TIR1-interaction properties, we reasoned to pinpoint the
175 determinants of these differences and the impact of IDRs on auxin-dependent
176 TIR1-AUX/IAA associations by creating 16 seamless IAA7 and IAA12 chimeric
177 proteins. We defined five different segments flanked by motifs conserved throughout

Niemeyer, M., et al

178 the AUX/IAA family: DI (N-terminus including KR motif), core degron (VGWPP-[VI]-
179 [RG]-x(2)-R), the PB1 domain (formerly known as DIII-DIV) and two variable IDRs
180 connecting either the DI and degron (linker), or the degron and PB1 domain (degron
181 tail) (**Fig. 2a, Supplementary Fig. 4**). We exchanged the modules between IAA7 and
182 IAA12 and used the resulting chimeras for interaction assays with TIR1 in the yeast-
183 two hybrid system (Y2H) for qualitative assessment of auxin co-receptor assembly
184 (**Fig. 2a, Supplementary Fig. 4**). TIR1 interacts in an auxin-dependent manner with
185 IAA7 containing all its native segments, denoted IAA(7-7-7-7-7). Expression of the β -
186 galactosidase reporter indicates stronger interaction of TIR1·IAA7 than TIR1·IAA12.
187 As expected, mimicking degron mutants *iaa7/axr2-1* (P87S) or *iaa12/bdl* (P74S) in the
188 IAA7 or IAA12 chimeras (7-7-7m-7-7, 12-12-12m-12-12) abolished their association
189 with TIR1 (**Fig. 2a**). Exchanging the disordered degron tail of IAA7 (36 aa) for the one
190 in IAA12 (49 aa) IAA(7-7-7-12-7) does not affect interaction with TIR1. A IAA(12-12-
191 12-12-7-12) chimera however, associated with TIR1 much more efficiently, and in an
192 auxin-dependent manner than wild type IAA(12-12-12-12-12). Similarly, PB1 domain
193 exchanges between IAA7 or IAA12 affected positively the ability of the IAA(12-12-12-
194 12-7) chimera to interact with TIR1. To investigate interdependency of the degron tail
195 and the PB1 domain, we exchanged the flexible degron tail of IAA12 together with its
196 corresponding PB1 domain, and fused them to IAA7 IAA(7-7-7-12-12). In this case,
197 TIR1·IAA(7-7-7-12-12) interaction is greatly affected, while TIR1·IAA(12-12-12-7-7)
198 interaction, although weak, remains stronger than TIR1·IAA(12-12-12-12-12)
199 association. Next, we omitted the degron tails in either the wild type proteins or in the
200 PB1-swapped versions. In both instances, when IAA7 lacks its native degron tail
201 irrespective of the PB1 it carries, (7-7-7- Δ -7 or 7-7-7- Δ -12) basal interactions with TIR1
202 do not occur and auxin-dependent interactions are greatly diminished. On the other

Niemeyer, M., et al

203 hand, IAA(12-12-12- Δ -12) and IAA(12-12-12- Δ -7) chimeras invariably exhibit an
204 increased ability to interact with TIR1, independently of their expression level
205 (**Supplementary Fig. 4**). Surprisingly, in each case when we omitted the PB1 domain
206 of IAA7 chimeras, we observed strong interactions with TIR1. This coincidentally
207 supports previous observations where removal of the folded PB1 domain in several
208 AUX/IAAs resulted in accelerated auxin-induced turnover²⁹. It has been postulated
209 this effect is due to high order complexes the PB1 domains engage in, which might
210 negatively influence AUX/IAA processing in yeast²⁹. Hence, when the PB1 domain is
211 omitted, chimeric proteins seem to be unhindered by oligomeric interactions and
212 readily interact with TIR1 in yeast. Of note, independently of the layout of the core
213 degron, either GWPPVR in IAA7 or GWPPIG in IAA12, the IAA7 degron tail and PB1
214 combo of IAA7 favor auxin-dependent TIR1·AUX/IAA chimera interactions
215 (**Supplementary Fig. 5**). Taking together, auxin-dependent and –independent
216 interactions are influenced by both the degron tail and the PB1 domain, as they
217 probably act in concert.

218 In order to address whether accessibility of IDRs and the PB1 domain in AUX/IAAs
219 affect the outcome of TIR1·AUX/IAA interactions, we carried out *in vitro* radioligand
220 binding assays. We used recombinant TIR1 as well as IAA7 and IAA12 chimeric or
221 *iaa7bm3* and *iaa12bm3* mutant proteins. While auxin binding affinities of
222 TIR1·*iaa7bm3* and TIR1·IAA(7-7-7-7-12) complexes are reduced when compared to
223 the TIR1·IAA7 co-receptor system (TIR1·*iaa7bm3* = K_d ~53 and TIR1·IAA(7-7-7-7-12)
224 = K_d 45 nM vs. TIR1·IAA7 K_d ~23 nM), we observed similar auxin affinities of
225 TIR1·*iaa12bm3* and TIR1·IAA12 co-receptors (K_d ~195 nM vs. 226 nM, respectively)
226 (**Fig. 2b-d, Supplementary Fig. 6**). This indicates that homotypic interactions in the
227 case of IAA12 might not interfere with the auxin binding properties of an IAA12-

Niemeyer, M., et al

228 containing auxin co-receptor. The decrease in the auxin binding affinity of
229 TIR1·iaa7bm3 and TIR1·IAA(7-7-7-7-12) co-receptors hints to a positive effect of the
230 IAA7 PB1 domain on auxin sensing (**Fig. 2b and d**). Exchange of disordered degron
231 tails in chimeric IAA7 and IAA12 altered the affinity for auxin. The degron tail of IAA12
232 in the IAA7 context, IAA(7-7-7-12-7), reduces by two-fold auxin binding affinity of the
233 receptor (**Fig. 2b-d**). Conversely, the disordered degron tail of IAA7 in an IAA12
234 context, IAA(12-12-12-7-12), appears to enhance AUX/IAA contribution to an auxin
235 receptor. This is consistent with our Y2H data, where we observed a unique positive
236 effect of the IAA7 PB1 domain. Taken together, our data confirm the postulated
237 interdependency of the degron tail and PB1 domain, and further point to additive and
238 separate effects of each disordered degron tail and the PB1 domain on auxin-
239 independent and auxin-triggered TIR1 interaction.

240

241 **IDRs in AUX/IAAs harbor ubiquitylation sites or facilitate their accessibility**

242 To investigate differences in ubiquitylation dynamics, and reveal whether the
243 disordered nature of IAA7 and IAA12 influences their ubiquitylation rate, we
244 recapitulated auxin-triggered and SCF^{TIR1}-dependent IAA7 and IAA12 ubiquitylation
245 ³¹. We traced IAA7 and IAA12 ubiquitylation over time and covered IAA concentrations
246 between the auxin binding affinity (K_d) of TIR1·IAA7 and TIR1·IAA12 co-receptor
247 complexes (*i.e.* 25 nM to 155 nM) (**Fig. 2d**) and at higher, saturating conditions (**Fig.**
248 **3, Supplementary Fig. 7**). Ubiquitin-conjugates on IAA7 and IAA12 were traceable
249 10 min after incubation, and their ubiquitylation is accelerated in an auxin-dependent
250 manner. We observed robust SCF^{TIR1}-mediated IAA7 ubiquitylation even in the
251 absence of auxin, which can be explained by previously reported basal TIR1·IAA7
252 interactions ²¹. IAA12~ubiquitin conjugates were much less abundant than IAA7 after

Niemeyer, M., et al

253 30 min incubation (**Fig. 3a**). Once an auxin concentration above the K_d for the
254 TIR1·IAA12 (± 150 nM) co-receptor complex is reached however, the differences in
255 ubiquitin conjugation on IAA7 and IAA12 are negligible over time. Reaching an auxin
256 concentration of 1 μ M corresponding to at least 50-times the K_d of TIR1·IAA7, and 4-
257 5-times the K_d of TIR1·IAA12 for IAA (**Fig. 2d**), AUX/IAA ubiquitylation becomes solely
258 time-dependent. We conclude IAA7 and IAA12 ubiquitylation occurs rapidly, and the
259 differences in ubiquitylation dynamics depend on the auxin binding affinity by their
260 corresponding receptors when in complex with TIR1. Given auxin to be a “molecular
261 glue” between TIR1·AUX/IAAs, we postulate auxin might be needed for increasing the
262 dwell-time of flexible AUX/IAAs on TIR1. This facilitates sampling of favorable
263 AUX/IAA conformations allowing efficient ubiquitin transfer to lysine residues.

264 Putative ubiquitin acceptor lysine residues along the IAA7 and IAA12 sequences are
265 enriched in the degron tail of IAA12, and the linker of IAA7, both of which appear to
266 lack a three dimensional (3D) structure (**Fig. 3b**). We aimed therefore at gaining
267 experimental evidence of IAA7 and IAA12 ubiquitylation sites, after *in vitro*
268 ubiquitylation (IVU) reactions, tryptic digest and LC/MS analysis. We were able to map
269 only few specific lysine residues on IAA7 and IAA12, which are differently distributed
270 along their sequence (**Fig. 3b, Supplementary Table 1**). Although IAA7 and IAA12
271 contain 24 and 18 lysine residues, respectively, only 3 and 6 of them were
272 ubiquitylated. While we observed only few ubiquitylated lysine residues at the AUX/IAA
273 N-terminus, most of the mapped ubiquitylation sites were located in the region
274 downstream of the degron, either in the PB1 domain in IAA7, or the degron tail in
275 IAA12. Even though 4 lysines are conserved in the PB1 domain of IAA7 and IAA12,
276 only the non-conserved residues appeared to be ubiquitylated in IAA7. The flexible
277 degron tail of IAA7 did not get ubiquitylated, whereas 4 out of 7 lysine residues in the

Niemeyer, M., et al

278 slightly longer disordered IAA12 degron tail could be mapped as ubiquitylation sites
279 (**Fig. 3b, Supplementary Table 1**).

280 To further investigate whether the apparent structural divergence of IAA7 and IAA12
281 imposes restrictions to lysine access for ubiquitylation, we used chimeric IAA7 and
282 IAA12 proteins (**Fig. 3c**) in our IVU assay. As we aimed at visualizing absolute
283 differences in ubiquitin conjugation, we traced auxin-dependent ubiquitin conjugation
284 of chimeric AUX/IAAs at a fixed IAA concentration of 0.5 μ M after 1 hour IVU reaction.
285 Exchanging the degron tails or the PB1 domains between IAA7 and IAA12 led to
286 differences in ubiquitylation profiles of chimeric proteins compared to their wild type
287 counterparts. This happens as we either added or subtracted regions that contain the
288 ubiquitin acceptor sites in the IAA7 and IAA12 chimeric proteins (**Fig. 3c,**
289 **Supplementary Fig. 8**). For instance, we detected an increase of ubiquitin conjugates
290 on IAA(7-7-7-12-7), which gains ubiquitylation sites due to the exchange of the IAA7
291 degron tail. Deleting the AUX/IAA degron tail or the PB1 domain in the chimeric
292 proteins results in an overall reduction of ubiquitin conjugates on targets. Versions of
293 IAA7 or IAA12 missing a degron tail and containing the PB1 domain of IAA12, IAA(7-
294 7-7- Δ -12) and IAA(12-12-12- Δ -12), do not undergo auxin-triggered ubiquitylation (**Fig.**
295 **3c, Supplementary Fig. 8**). Similarly, AUX/IAA versions containing the IAA7 degron
296 but lack a PB1 domain (IAA(7-7-7-7- Δ), IAA(12-12-12-7- Δ)) are not conjugated by
297 ubiquitin, probably due to the loss of the mapped ubiquitin acceptor sites (**Fig. 3b**).
298 Our IVU assays on AUX/IAA chimeras validate our findings showing that the IAA7 PB1
299 domain or the flexible IAA12 degron tail carry propitious ubiquitylation sites. Thus, we
300 postulate AUX/IAA ubiquitylation favorably occurs in exposed regions in IAA7 and
301 IAA12, when they are recruited by TIR1.

302

Niemeyer, M., et al

303 **TIR1-AUX/IAA ensembles are guided by the degron, but tailored by flexible**
304 **degron flanking regions**

305 Due to the relative lack of a stable 3D conformation, IDPs or proteins enriched in IDRs,
306 such as AUX/IAAs, represent a challenge for structural biology studies. During
307 interactions with target proteins, IDPs, particularly IDRs, may undergo conformational
308 changes that cannot be traced easily, or captured while happening^{35,36}. Although the
309 *Arabidopsis* SKP1 (ASK1)·TIR1·auxin·degron crystal structure enlightened us on how
310 auxin is perceived, we lack information on the contribution of regions flanking the
311 AUX/IAA degron on auxin binding. Thus, without being able to structurally resolve
312 intrinsically disordered degron flanking regions, we are hindered in our understanding
313 of how AUX/IAA ubiquitylation targets are actually positioned on TIR1. This has
314 evidently far-reaching implications on SCF^{TIR1} E3 ubiquitin ligase activity and ubiquitin
315 transfer by an E2 ubiquitin conjugating enzyme.

316 We aimed to elucidate the driving factors for ASK1·TIR1·AUX/IAA complex assembly
317 and to unveil how IDRs in AUX/IAAs influence positioning on TIR1. We pursued a
318 structural proteomics approach using chemical cross-linking coupled to mass
319 spectrometric analyses (XL-MS) (**Fig. 4a**). We assembled ASK1·TIR1·AUX/IAA
320 complexes containing either IAA7bm3 or IAA12bm3 proteins in the absence or
321 presence of auxin (IAA), and added the MS-cleavable cross-linker disuccinimidyl
322 dibutyric urea (DSBU). Reaction products were processed for mass spectrometric
323 analysis, which utilizes the characteristic fragmentation of DSBU to identify cross-
324 linked residues within the AUX/IAAs and the ASK1·TIR1·AUX/IAA complex³⁷⁻³⁹. Our
325 data shows multiple intra- and inter-molecular cross-links for ASK1·TIR1 and IAA7bm3
326 or IAA12bm3 proteins in the presence of auxin (**Fig. 4b-d, Supplementary Fig. 9-10**).
327 In the absence of auxin, we observed only a few inter-protein and similar intra-protein

Niemeyer, M., et al

328 cross-links when compared to auxin-containing samples (**Fig. 4, Supplementary Fig.**
329 **10**). In the presence of auxin, we identified two distinct clusters in TIR1 harboring
330 cross-linker-reactive amino acid side chains with IAA7 and IAA12 (**Fig. 4b,**
331 **Supplementary Fig. 9**). Cluster 1 comprises amino acid residues in LRR7 (217-229
332 aa), while cluster 2 consists of residues toward the TIR1 C-terminus located in LRR17-
333 18 (485-529 aa). The location of the clusters on two opposing surfaces of TIR1
334 suggests a rather extended fold of the AUX/IAA protein when bound to TIR1 (**Fig. 4b**).
335 The cross-linked residues along the sequences of ASK1·TIR1·IAA7bm3 or
336 ASK1·TIR1·IAA12bm3 show an enrichment of highly variable intra-molecular cross-
337 links within the AUX/IAAs (**Fig. 4c-d**). A low number of intra-protein cross-links along
338 the TIR1 sequence were detected as a consequence of its rigid solenoid fold, which
339 is in agreement with the ASK1·TIR1 crystal structure (PDB: 2P1Q, ²⁰). Inter-protein
340 cross-links indicate that the cross-linker-reactive clusters in TIR1 mainly connect with
341 only a specific subset of AUX/IAA residues (**Fig. 4b**). Multiple IAA7 residues upstream
342 of the core degron, including the KR motif, preferably cross-linked to TIR1 cluster 2.
343 While residues downstream of the core degron, including the PB1 domain, positioned
344 towards TIR1 cluster 1 (**Fig. 4c**). IAA12 is similarly positioned on TIR1, but exhibits
345 even higher flexibility given the more diverse distribution of inter-protein cross-links
346 (**Fig. 4d**). This is also supported by the fact that we detected many more assemblies
347 for ASK1·TIR1·IAA12bm3 across replicates, than for the ASK1·TIR1·IAA7bm3
348 complex (**Fig. 4c-d**). In conclusion, our structural proteomics approach confirmed
349 AUX/IAAs IAA7 and IAA12 exhibit flexible conformations in solution (intra-protein
350 cross-links), and adopt an extended fold when bound to TIR1.

351 As we gained a better understanding on the extended fold of IAA7 and IAA12 on TIR1,
352 we wondered whether intrinsic disordered stretches flanking the degron might help to

Niemeyer, M., et al

353 coordinate positioning of the folded PB1 domain. An extended AUX/IAA configuration
354 on TIR1 would be particularly relevant for allowing K146 and K223 in the PB1 domain
355 of IAA7 to be readily available for ubiquitylation. In the case of IAA12, an assertive
356 extension of the degron tail would expose K91, K111, K116 and K120 for ubiquitin
357 attachment (**Fig. 3b**).

358

359 **Conformational heterogeneity in flexible IDR steers AUX/IAA molecular** 360 **interactions**

361 To further investigate how the intrinsic disorder in IAA7 and IAA12 influence their
362 positioning on ASK1·TIR1, we combined our cross-linking information with a molecular
363 docking strategy (**Fig. 5, Supplementary Fig. 11**). For that, we use available
364 structures for the PB1 domains of AUX/IAAs and ARFs⁴⁰⁻⁴³. We docked homology-
365 modeled PB1 domains of *Arabidopsis* IAA7 and IAA12 to the ASK1·TIR1 complex,
366 applying distance restraints based on the cross-linking data (**Fig. 5, Supplementary**
367 **Fig. 11**). We also added an additional distance restraint reflecting the possible
368 conformational space covered by the respective degron tails. We visualized the impact
369 of the different restraints on the possible interaction interface of ASK1·TIR1·IAA7^{PB1}
370 and ASK1·TIR1·IAA12^{PB1} by DisVis⁴⁴ (**Fig. 5c-d**). Evidently, by incorporating more
371 distance restraints, we limit the number of ASK1·TIR1·AUX/IAA^{PB1} protein complexes,
372 therefore reducing their explored interaction space (**Fig. 5**).

373 Intriguingly, the relationship between the number of accessible complexes vs. the
374 number of restraints applied does not reveal a linear behavior, but shows a sharp drop
375 when the degron tail restraint is added to all cross-link-based restraints (**Fig. 5a-b**).

376 Comparing the groups of water-refined HADDOCK models lead to similar observations

Niemeyer, M., et al

377 and the best scoring groups were only sampled incorporating the degron tail restraint
378 (**Supplementary Table 2**). This indicates the disordered degron tail restricts the
379 conformational space explored by the PB1 domain (**Supplementary Table 2,**
380 **Supplementary Fig. 11-12**). The reduction of accessible ASK1·TIR1·IAA7^{PB1} and
381 ASK1·TIR1·IAA12^{PB1} complexes for docking is also reflected by the decreased space
382 that can be possibly occupied by the PB1 domain (**Fig. 5c-d**). Overall, cross-linking-
383 based docking of the PB1 domain of IAA12 on the ASK1·TIR1 complex is less-defined,
384 and occupies a distinct conformational space than the ASK1·TIR1·IAA7^{PB1} complex.

385 In order to refine our docking data and identify the most energetically-favored
386 TIR1·AUX/IAA^{PB1} assemblies, we carried out molecular dynamic simulations coupled
387 to free-binding energy calculations by MM/GBSA. We used as a starting structure (t=0)
388 the results from the HADDOCK simulations including the degron tail restraint, and
389 performed 20 ns simulations for each TIR1·IAA7^{PB1} or TIR1·IAA12^{PB1} complex (**Fig. 6**
390 **a-b**). We obtained the effective binding free energy every 1 ps for each simulation,
391 and observed distinct average effective energy (ΔG_{eff}) for the different groups in each
392 system (protein complex). Group 1 for TIR1·IAA7^{PB1} and groups 1 and 3 for
393 TIR1·IAA12^{PB1} turned out to be energetically less favored, while groups 2 in each case
394 showed the lowest binding energy. This indicates groups 2 likely depict the most
395 probable ensembles (**Fig. 6 a-b**). To identify relevant residues in groups 2 favoring
396 TIR1·AUX/AA interactions, we carried out per-residue effective energy decomposition
397 analysis (prEFED) followed by validation via computational alanine scanning (CAS)
398 (**Fig. 6c, Supplementary Table 3**). We found residues in TIR1 that might engage in
399 polar interactions with the AUX/IAA PB1 domain. D119, D170, V171, S172, H174,
400 H178, S199, R220 along the LRR3-6 in TIR1 likely contribute to stabilization of the
401 TIR1·IAA7 PB1 complex. Residues H174, H178, S199 also stabilized TIR1·IAA12 PB1

Niemeyer, M., et al

402 interactions together with R156, S177, S201, and R205 in TIR1 LRR4-6 (**Fig. 6c-d**,
403 **Supplementary Fig. 13**).

404 Next, we assessed empirically whether the *in silico* identified TIR1 residues contribute
405 to TIR1·AUX/IAA interaction. We generated mutant TIR1 proteins and evaluated their
406 interaction with either ASK1 or IAA7 and IAA12 in Y2H assays (**Fig. 6e**). We aimed at
407 identifying residues in cluster 1 at the TIR1 NTD and cluster 2 in TIR1 CTD (**Fig. 4b**),
408 which might provide non-native interaction interfaces with either the PB1 domain or
409 the KR motif of AUX/IAA proteins, respectively (**Fig. 6c-e, Supplementary Table 3**).
410 Mutations R156E, as well as S201A, and S205A either abolished or drastically
411 impaired basal TIR1·IAA7 and auxin-driven TIR1·IAA7 and TIR1·IAA12 associations,
412 without affecting ASK1·TIR1 assembly. This allowed us to postulate that the
413 positioning of the PB1 domain of AUX/IAAs on a specific NTD region in TIR1 might
414 have a favorable effect as part of the target recruitment mechanism. Specifically, IAA7
415 and IAA12 PB1 “piggy tails” might be in contact with R156 in TIR1. On the other hand,
416 mutations S172A, H174A, E197A, S199A, and R220A impaired ASK1·TIR1 and
417 TIR1·IAA7, as well as TIR1·IAA12 interactions. This data suggests these mutations
418 causing a long range effect on TIR1 activity and probably its overall conformational
419 stability, that is however independent on TIR1 expression levels (**Fig. 6f**). While D170
420 offered one of the best CAS scores (**Supplementary Table 3**), D170K mutation
421 probably corresponds to a null allele, as it leads to a reduction of protein levels, and a
422 complete disruption of TIR1 associations (**Fig. 6c, e-f**).

423 Among the mutants tested, we also included a reversed charge exchange for D481,
424 which is located in a negative charged patch in cluster 2 of TIR1 (**Fig. 4b**). According
425 to our cross-linking data, this exposed patch (*incl.* D481, S482, E459 or E506) might
426 exert electrostatic interactions with a conserved Lys-Arg (KR) dipeptide located

Niemeyer, M., et al

427 between the AUX/IAA N-terminus and the degron (**Supplementary Fig. 9**). The KR
428 was previously postulated to act as auxin-responsive rate motif influencing AUX/IAA
429 turnover, and the magnitude of this effect was correlated with the proximity of the KR
430 to the degron ^{28,29}. Interestingly, we found evidence for the KR motif in AUX/IAAs to
431 favor basal interactions with the CTD of TIR1, as D481R abolished TIR1·IAA7
432 interaction in the absence of auxin, while weakening auxin-driven TIR1·IAA7 and
433 TIR1·IAA12 interactions (**Fig. 6e**).

434 Our interaction studies combined with a structural proteomics approach demonstrated
435 IDRs in IAA7 and IAA12 harbor specific features that support TIR1·AUX/IAA
436 interactions. Charged residues surrounding the KR motif, the core degron, the degron
437 tail and the PB1 domain act in concert to secure AUX/IAA on TIR1, thereby modulating
438 auxin binding dynamics and likely enabling efficient ubiquitin transfer.

Niemeyer, M., et al

439 Discussion

440 Auxin is perceived by the FBP TIR1 and its ubiquitylation targets the AUX/IAA
441 transcriptional repressors. While TIR1 adopts a compact solenoid fold, AUX/IAAs
442 appear flexible and modular in nature as they engage in various protein interaction
443 networks^{23,45}. A 13-aa degron motif in AUX/IAAs seals a ligand binding groove in
444 TIR1, securing auxin in place. To date, we lacked information on whether additional
445 physical interactions between TIR1-AUX/IAAs influence conformation and fate. We
446 also did not know whether additional partner interactions facilitate the formation of the
447 final auxin receptor complex by a two-dimensional search on the part of TIR1 on the
448 AUX/IAA surface or *vice versa*. We found IAA7 and IAA12 exhibit conformational
449 flexibility due to the presence of IDRs along their sequence. From the TIR1-auxin-IAA7
450 degron structure, we observed the degron adopts a slight helical structure²⁰. Our data
451 shows this semihelical peptide is embedded in an intrinsically disordered stretch,
452 which represent ~50% of the AUX/IAA sequence, and winds down in the well-folded
453 PB1 domain.

454 We showed IAA7 and IAA12 have properties of a molten globule, or a loosely packed
455 and highly dynamic conformational fold. Although IAA7 and IAA12 might exhibit
456 conformational heterogeneity, we observed that, while in solution, they maintain
457 unprecedented flexibility that seems to favor recruitment by the SCF^{TIR1}.
458 Computational and experimental studies have shown IDRs such as those in
459 AUX/IAAs, act as inter-domain linkers contributing to protein-protein interactions by
460 exclusively or partially forming binding interfaces^{15,46,47}. Indeed ensembles of IAA7
461 and IAA12 with TIR1 captured by XL-MS allowed us to visualize AUX/IAAs “kissing
462 and embracing” TIR1 (**Fig. 7**). While the degron drives auxin-mediated interactions,
463 the IDR upstream of the degron and the PB1 domain engage in transient interactions

Niemeyer, M., et al

464 with the CTD, and the NTD of TIR1, respectively. A directional embrace of TIR1 by an
465 open-armed AUX/IAA, strengthened by degron-flanking IDRs, is initiated by a
466 TIR1-auxin-degron kiss or *vice versa*. This is remarkable indeed, as we show for the
467 first time that the PB1 domain may contact the TIR1 surface.

468 Signaling proteins carrying IDRs with mostly polar and charged residues seem to have
469 evolved more rapidly than ordered sequences, allowing increased functional
470 complexity^{48,49}. In our study, this applied to IDRs in regions upstream of the degron,
471 but not for AUX/IAAs degron tails. Although IAA7 and IAA12 show differences on IDR
472 content and length, both embraced TIR1 in a similar manner. Despite the fact that the
473 degron tail in IAA12 is third longest in the AUX/IAA family (49 aa) and about ~1.3 times
474 longer than the tail of IAA7 (36 aa), both offer flexibility (**Supplementary Fig. 14**). An
475 introduced degron length constraint in IAA7 and IAA12 greatly reduced the sampled
476 conformational space of IAA7 and IAA12 on TIR1. Finally, degron tails seem to
477 increase the interaction surface with TIR1, which we anticipate translates into
478 variability of binding kinetics.

479 Within the *Arabidopsis* AUX/IAA protein family, nearly half of the degron tails are
480 between 20-40 aa long and show high disorder probability (**Supplementary Fig. 1**).
481 Seven of the 23 degron-containing AUX/IAAs (IAA19, IAA4, IAA6, IAA5, IAA1, IAA2,
482 IAA15), however, carry a relatively ordered degron tail shorter than 20 amino acids
483 (**Supplementary Fig. 14**). Is that specific length an evolutionary constraint for TIR1
484 association? Auxin-dependent gene regulation, and AUX/IAA proteins appear in the
485 land plant lineage over 500 mya^{33,50}. When comparing the proteins sequence of the
486 two ancestral AUX/IAAs in moss and *Marchantia*^{25,26}, we observed their degron tails
487 are not much longer than the average degron tails (40 aa) of *Arabidopsis* AUX/IAAs,
488 despite the overall length of these proteins being at least double that of angiosperm

Niemeyer, M., et al

489 AUX/IAAs. It will be interesting to investigate whether degron tails length and disorder
490 content are a deeply conserved features for surface availability, and whether short
491 degron tails (less than 20 aa) can still offer tailored positioning on TIR1. Furthermore,
492 the degron tail might generate an entropic force ^{51,52} that is fine-tuned, but also
493 restricted by IDR length, modulating binding of AUX/IAAs to TIR1.

494 Particular stretches of amino acids with increased evolutionary conservation within
495 disordered segments have been found to determine interaction specificity, acting as
496 functional sites ^{48,49,53}. This seems to precisely apply to the region in AUX/IAAs
497 upstream of the degron containing the auxin-responsive rate KR motif ^{28,54}. The KR
498 exhibits a high level of conservation, and in addition to being part of a bipartite nuclear
499 localization signal (NLS), the KR contributes to assembly of a TIR1·AUX/IAA auxin
500 receptor complex and, probably as a result, is required for basal proteolysis *in planta*
501 and AUX/IAA degradation dynamics ^{21,28,29,54}. How mechanistically could the KR exert
502 an effect on TIR1 recognition and further AUX/IAA processing? Our findings lead us
503 to propose an answer to a more than 10 year's long standing question. As part of the
504 AUX/IAA embrace of TIR1, the KR motif embedded in the IDR upstream of the degron
505 offers alternative contacts with the CTD of TIR1 and probably first binding contacts
506 (**Fig. 7**). Previous studies showed that moving the KR motif closer to the degron was
507 not sufficient to accelerate AUX/IAA degradation rate ²⁹. We predict a high flexibility of
508 the IDR offers a necessary distance between the KR and the core degron for reaching
509 distinct TIR1 contact sites. So, the positively charged KR motif in AUX/IAAs may be
510 capable of engaging in electrostatic interactions with a cluster of highly charged (Asp,
511 Glu) residues in TIR1 between LRR16 and LRR18, where D481 is located. While TIR1
512 and AFB1 offer similar contact points to the KR in AUX/IAAs, AFB2 and AFB3 exhibit
513 opposite charged residues (Lys) that however might still provide charge-charge

Niemeyer, M., et al

514 interactions with a specific subset of AUX/IAAs. It remains to be determined whether
515 this is an additional feature facilitating differential auxin sensing by distinct
516 TIR1/AFBs-AUX/IAA co-receptor combinations ²¹.

517 Local flexibility in AUX/IAAs is evidently shaping their conformation when in complex
518 with TIR1. Specifically, flexible IDRs flanking the core degron in AUX/IAAs, as shown
519 for IAA7 and IAA12, serve as variable spacers between the degron and the well-folded
520 PB1 domain. Our data provide evidence for dynamic allosteric modulation of a
521 TIR1-AUX/IAA auxin receptor complex by the folded-PB1 domain and IDRs in
522 AUX/IAAs. We could track positive but also negative cooperativity, due to the degron
523 tail and PB1 domain combo, fine-tuning conformational states of TIR1-IAA7 and
524 TIR1-IAA12 receptor pairs, respectively. Further long-range, probable allosteric,
525 effects are reflected into AUX/IAA turnover, when PB1 domain and degron tail act as
526 one element (**Supplementary Fig. 5**).

527

528 Structural disorder in AUX/IAA targets appears also to be instrumental for processivity
529 in ubiquitin transfer by the SCF^{TIR1} E3 ubiquitin ligase. This is crucial as once an active
530 E2-E3-target assembly has formed, spatial and geometric constraints such as
531 distance and orientation relative to the E3-bound primary degron limit ubiquitylation
532 surface and lysine selection for degradation ⁷. AUX/IAA sequence harbors a number
533 of putative ubiquitin acceptor lysines (~9% total sequence) (**Supplementary Fig. 14**).
534 Our data show that not all of these sites are favorable for ubiquitylation. Downstream
535 of the core degron, AUX/IAAs likely offer an attractive region for ubiquitin conjugation.
536 We predict either the PB1 or the degron tail facilitate the accessibility of receptor
537 residues that undergo ubiquitylation. Upon TIR1-AUX/IAA interaction, IDRs either act
538 themselves as ubiquitylation acceptor sites (e.g. IAA12) or orient the PB1 domain-

Niemeyer, M., et al

539 located lysines as ubiquitin acceptor sites (e.g. IAA7). We cannot rule out however,
540 regulated and efficient ubiquitin transfer might prioritize target degradation at the
541 proteasome. This is key, as AUX/IAA turnover likely needs properly positioned
542 ubiquitin moieties at the proper distance of an IDR, and an IDR with unbiased
543 sequence composition as an initiation site for efficient degradation ⁵⁵⁻⁵⁷. To better
544 understand this, it will be imperative to gain insights into where AUX/IAAs are
545 ubiquitylated *in vivo*, and where exactly the proteasome initiates degradation relative
546 to the ubiquitylation sites.

547 The effects of cooperative allostery driven by IDRs in AUX/IAA proteins might not be
548 limited to the TIR1-AUX/IAA interaction, but rather influence the assembly into other
549 complexes regulating auxin output signals ⁵⁸. It is therefore also possible that in
550 response to fluctuating cellular auxin concentrations, transient TIR1-AUX/IAA
551 interactions via IDRs alter the energy landscape of AUX/IAA-TPL, AUX/IAA-ARF and
552 AUX/IAA-AUX/IAA assemblies and/or possible decorations with PTMs. Future studies
553 will tell whether IDRs in AUX/IAAs, and the recently described IDRs in ARFs, affect
554 their protein assembly's localization or activity ⁵⁹. One can envision, IDR-driven
555 cooperativity resulting in a multiplicity of allosterically-regulated interactions within the
556 auxin signaling pathway, where AUX/IAAs act as signaling hubs within the different
557 complexes.

558 Using an XL-MS approach, we have captured for the first time a highly flexible
559 ubiquitylation target being engaged by an SCF-type E3 ubiquitin ligase, which at the
560 same time, constitutes a phytohormone receptor. Our strategy offers an opportunity to
561 visualize how IDR-driven allostery might influence a complex signaling network.

Niemeyer, M., et al

562 **Methods**

563 **Phylogenetic tree generation and secondary structure analysis**

564 Phylogenetic tree construction was done using Clustal Omega⁶⁰ with standard settings
565 and the full-length protein sequences of all *Arabidopsis* AUX/IAAs deposited at
566 uniprot⁶¹. The constructed tree was visualized by iTOL⁶² and manually edited. *In silico*
567 disorder analysis was performed with the web-based IUPred2A tool³² utilizing
568 AUX/IAA protein sequences. The resulting disorder probability was used to categorize
569 each residue as either ordered (<0.4), intermediate (0.4-0.6) or disordered (>0.6).
570 Same analysis was done for all AUX/IAA proteins excluding the PB1 domain using the
571 conserved VKV motif as the start of the PB1 domain. Residues of each category were
572 plotted using R. IAA7 and IAA12 disorder predictions were additionally carried out
573 using SPOT⁶³ and PrDOS⁶⁴ algorithms with standard settings. Hydropathy plots were
574 generated via ExPASy-linked ProtScale^{65,66} using the Kyte-Doolittle method⁶⁷.

575

576 **Protein purification**

577 ASK1-TIR1 complex was purified from Sf9 cells as described earlier²⁰ with minor
578 changes. In brief, ASK1 was co-purified with GST-TIR1 using GSH affinity
579 chromatography (gravity flow) and anion chromatography (MonoQ) followed by Tag-
580 removal and a final size-exclusion chromatography (SEC) step (Superdex 200), using
581 an ÄKTA FPLC system.

582 AUX/IAA proteins, including chimeric versions, were expressed as GST-tagged
583 proteins in *E.coli* and purified using GSH affinity chromatography, including a high salt
584 wash (1M NaCl) and gravity flow anion exchange chromatography (Sepharose Q). For
585 circular dichroism, the GST-tag was removed on the GSH column matrix with
586 thrombin, and fractions containing AUX/IAAs were briefly concentrated, passed over

Niemeyer, M., et al

587 a benzamidine column, and further purified using a Sephacryl S100 column (SEC)
588 with an ÄKTA FPLC system. This step was carried out using the CD measurement
589 buffer (see CD measurement section) for buffer exchange.

590

591 **Size exclusion chromatography and size calculations**

592 The last protein purification step was used to simultaneously determine the Stokes
593 radii of AUX/IAAs in CD buffer (10 mM KPi pH 7.8; 150 mM KF; 0.2 mM TCEP). The
594 HiPrep 16/60 Sephacryl S-100 high resolution column was calibrated using gel
595 filtration standards (Bio-Rad, Cat. #151-1901) with added BSA before the runs. Stokes
596 radii for the globular known reference proteins were calculated as described⁶⁸. The
597 Stokes radii of AUX/IAA variants were calculated from the resulting calibration curve
598 equation based on their retention volume (n = 4-9).

599

600 **Circular Dichroism (CD) measurements**

601 After purification, including tag-removal and size exclusion chromatography,
602 AUX/IAAs were concentrated and adjusted to 2.5 - 5 μ M in CD buffer. CD
603 measurements were carried out on a Jasco CD J-815 spectrometer and spectra were
604 recorded from 260 nm to 185 nm as 32 accumulations using a 0.1 nm interval and 100
605 nm/min scanning speed. Cell length was 1 mm and temperature was set to 25°C. All
606 spectra were buffer corrected using CD buffer as a control and converted to mean
607 residual ellipticity (MRE). Reference spectra for a disordered (MG-14; PCDDDBID:
608 CD0004055000), a beta-sheet (BtuB; PCDDDBID: CD0000102000) and an alpha-
609 helical protein (amtB; PCDDDBID: CD0000099000) were used.

610

611 **[3H]-labeled Auxin Binding Assay**

Niemeyer, M., et al

612 Radioligand binding assays were performed as previously described⁶⁹ using purified
613 ASK1-TIR1 protein complexes, GST-tagged AUX/IAAs incl. chimeric AUX/IAAs and
614 [³H]IAA with a specific activity of 25 Ci/mmol (Hartmann Analytic). Final protein
615 concentrations in a 100 μ L reaction were 0.01 μ M ASK1-TIR1 complex and 0.3 μ M
616 AUX/IAAs. Complexes were allowed to form 1 h on ice, shaking. For non-specific
617 binding controls, reactions contained additionally 2 mM cold IAA. Data was evaluated
618 with GraphPad Prism v 5.04, and fitted using the “one site total and non-specific
619 binding” preset.

620

621 **LexA Yeast Two Hybrid Assays**

622 LexA-based yeast two hybrid assays were performed using yeast transformed with the
623 described constructs (DBD-fusions: EGY48+pSH18-34, pGILDA vector; AD-fusions:
624 YM4271, pB42AD vector), freshly mated and grown on selection medium (Gal/Raff –
625 Ura –His –Trp). Same amount of yeast cells ($OD_{600} = 0.4$ or 0.8 for IAA12(-like)) were
626 spotted on selection plates containing BU salts (final: 7 g/L Na_2HPO_4 , 3 g/L NaH_2PO_4 ,
627 pH 7), X-Gal (final 80 mg/L) and the given auxin (IAA) concentration. Plates were
628 incubated at 30°C for several days and constantly monitored. Expression of chimeric
629 AUX/IAAs and TIR1 mutants in yeast were checked using immunoblot analysis on
630 lysates from haploid yeast. 50 mL liquid selection medium (Gal/Raff -Ura -His or -Trp)
631 were inoculated with an 1/25 volume overnight culture and grown till $OD_{600} \approx 0.6$,
632 harvested, washed with water and lysed in 200 μ L lysis buffer (0.1 M NaOH, 2 % β -
633 mercaptoethanol, 2 % sodium dodecyl sulfate, 0.05 M EDTA, 200 μ M benzamidine, 1
634 mM PMSF, Roche protease inhibitor cocktail) at 90°C for 10 min. After neutralization
635 with 5 μ L 4 M sodium acetate for 10 min at 90°C, 50 μ L 4X Laemmli was added and
636 samples were separated via SDS-PAGE and immunoblotted.

Niemeyer, M., et al

637 **In vitro reconstitution of Ub-conjugation**

638 *In vitro* ubiquitylation (IVU) reactions were performed as previously described³¹. In
639 brief two protein mixtures (mix A and mix B) were prepared in parallel. Mix A contained
640 50 μ M ubiquitin (Ub; Fluorescein-labeled Ub^{S20C}: Ub^{K0}; 4:1 mix), 0.2 μ M 6xHis-UBA1
641 (E1) and 2 μ M 6xHis-AtUBC8 (E2) in reaction buffer (30 mM Tris-HCl, pH 8.0, 100 mM
642 NaCl, 2 mM DTT, 5 mM MgCl₂, 1 μ M ZnCl₂, 2 mM ATP). Mix B contained 1 μ M
643 Cul1·RBX1, 1 μ M ASK1·TIR1, and 5 μ M AUX/IAA protein in reaction buffer. Mix B was
644 aliquoted and supplemented with IAA to reach the indicated final concentration.
645 Mixtures A and B were separately incubated for 5 or 10 minutes at 25 °C, respectively.
646 Equal volumes of mix A and B were combined, aliquots were taken at specified time
647 points, and reactions were stopped by denaturation in Laemmli buffer. IVUs with
648 chimeric AUX/IAAs were carried out 1 h with 1 μ M IAA. Immunodetection of Ub-
649 conjugated proteins was performed using polyclonal anti-GST in rabbit (Sigma,
650 G7781; 1:20,000) antibodies combined with secondary anti-rabbit Alexa Fluor® Plus
651 647 antibody (1:20,000) (Thermo Fischer Scientific, A32733). Detection was
652 performed with a Typhoon FLA 9500 system (473 nm excitation wavelength and LPB
653 filter for fluorescein-labeled ubiquitin signal detection and 635 nm excitation
654 wavelength and LPR filter for GST signal).

655 Quantification of ubiquitylated AUX/IAAs was performed using the in-gel fluorescein
656 signal above GST-IAA7 and GST-IAA12, as well as the ubiquitin-modified Cullin (~50
657 kDa) were quantified for each lane using ImageQuant TL software automatic lane
658 detection. The reduction of unmodified GST-IAA7 and GST-IAA12 fusion proteins was
659 quantified after blotting and immunodetection using the Alexa Fluor 647 signal, and
660 automatic band detection. All signals were background subtracted (rubberband
661 method).

Niemeyer, M., et al

662 **LC-MS analyses of IVU reactions**

663 Three sets of IVUs, corresponding to three biological replicates, were carried out on
664 consecutive weeks using AUX/IAA proteins from different batch preparations. After 30
665 minutes, IVUs were stopped by denaturing with urea, reduced with DTT and alkylated
666 with iodoacetamide. Trypsin digestion was carried out overnight at 37°C. Upon
667 quenching and desalting, peptides were separated using liquid chromatography C18
668 reverse phase chemistry and later electrosprayed on-line into a QExactive Plus mass
669 spectrometer (Thermo Fisher Scientific). MS/MS peptide sequencing was performed
670 using a Top20 DDA scan strategy with HCD fragmentation. Ubiquitylated residues on
671 identified peptides were mapped using GG and LRGG signatures (as tolerated
672 variable modifications) from using both the Mascot software v2.5.0 (Matrix Science)
673 linked to Proteome Discoverer v1.4 (Thermo Fisher Scientific) and the MaxQuant
674 software v1.5.0.0. Mass spectrometry proteomics data are being currently curated at
675 PRIDE repository, ProteomeXchange (<http://www.ebi.ac.uk/pride/archive/>). A dataset
676 identifier will be shared upon acceptance of the manuscript.

677

678 **Cross-linking reactions**

679 DSBU (ThermoFisher) cross-linking reactions were performed for 1 h at 25°C with
680 either 4-5 µM of ASK1-TIR1 and 5 µM iaa7bm3 or iaa12bm3 or 10 µM iaa7bm3 or
681 iaa12bm3 alone. Proteins were pre-incubated 15 minutes in the presence or absence
682 of 10 µM auxin (IAA) before addition of 1 mM DSBU (100 molar excess). After TRIS
683 quenching, samples were sonicated in the presence of sodium deoxycholate, reduced
684 with DTT, and alkylated with iodoacetamide. Alkylation was quenched by DTT, and
685 the reactions were incubated with trypsin over night at 37°C. Digestion was stopped

Niemeyer, M., et al

686 with 10% TFA and after centrifugation (5 min 14.000 xg), peptide mixtures were
687 analyzed via LC/MS.

688

689 **Mass spectrometry analyses of cross-linked peptides & data analysis**

690 Proteolytic peptide mixtures were analyzed by LC/MS/MS on an UltiMate 3000 RSLC
691 nano-HPLC system coupled to an Orbitrap Fusion Tribrid mass spectrometer (Thermo
692 Fisher Scientific). Peptides were separated on reversed phase C18 columns (trapping
693 column: Acclaim PepMap 100, 300 μm \times 5 mm, 5 μm , 100 \AA (Thermo Fisher Scientific);
694 separation column: self-packed Pico frit nanospray C18 column, 75 μm \times 250 mm, 1.9
695 μm , 80 \AA , tip ID 10 μm (New Objective)). After desalting the samples on the trapping
696 column, peptides were eluted and separated using a linear gradient from 3% to 40%
697 B (solvent A: 0.1% (v/v) formic acid in water, solvent B: 0.08% (v/v) formic acid in
698 acetonitrile) with a constant flow rate of 300 nl/min over 90 min. Data were acquired in
699 data-dependent MS/MS mode with stepped higher-energy collision-induced
700 dissociation (HCD) and normalized collision energies of 27%, 30%, and 33%. Each
701 high-resolution full scan (m/z 299 to 1799, $R = 120,000$ at m/z 200) in the orbitrap was
702 followed by high-resolution product ion scans ($R = 30,000$), starting with the most
703 intense signal in the full-scan mass spectrum (isolation window 2 Th); the target value
704 of the automated gain control was set to 3,000,000 (MS) and 250,000 (MS/MS),
705 maximum accumulation times were set to 50 ms (MS) and 200 ms (MS/MS) and the
706 maximum cycle time was 5 s. Precursor ions with charge states $<3+$ and $>7+$ or were
707 excluded from fragmentation. Dynamic exclusion was enabled (duration 60 seconds,
708 window 2 ppm).

709 For cross-linking analysis, mass spectrometric *.raw files were converted to mzML
710 using Proteome Discoverer 2.0. MeroX analysis was performed with the following

Niemeyer, M., et al

711 settings: Proteolytic cleavage: C-terminal at Lys and Arg with 3 missed cleavages,
712 peptides' length: 5 to 30, static modification: alkylation of Cys by IAA, variable
713 modification: oxidation of M, cross-linker: DSBU with specificity towards Lys, Ser, Thr,
714 Tyr, and N-termini, analysis mode: RISE-UP mode, minimum peptide score: 10,
715 precursor mass accuracy: 3 ppm, product ion mass accuracy: 6 ppm (performing mass
716 recalibration, average of deviations), signal-to-noise ratio: 1.5, precursor mass
717 correction activated, prescore cut-off at 10% intensity, FDR cut-off: 1%, and minimum
718 score cut-off: 60. For further analysis only cross-links found in at least 2/3 (IAA7) or
719 3/4 (IAA12) experiments were considered.

720

721 **Cross-link-based docking using HADDOCK**

722 Comparative models of IAA7 and IAA12 PB1 domains were created using multi-
723 sequence-structure-alignments (PIR formatted) as input for MODELLER 0.921⁷⁰. The
724 generated models were incorporated for the HADDOCK-based docking together with
725 the available ASK1·TIR1 structure (PDB code: 2P1Q, resolution: R= 1.91 Å)²⁰. A
726 detailed description how to prepare pdb files and incorporated distance restraint can
727 be found elsewhere. Formatted pdb files were uploaded to the HADDOCK server^{71,72}
728 using guru access level. To incorporate distance restraints, we used distances from
729 intramolecular cross-links of known distance (see SUPP file docking parameters). We
730 further added a distance restraint or not corresponding to the degron tail length
731 calculated as described⁷³. For each complex docked, 10,000 rigid body docking
732 structures were generated followed by a second iteration (400 best structures). Finally,
733 200 models/structures were water refined (explicit solvent) and clustered (FCC⁷⁴ at
734 0.6 RMSD cutoff).

Niemeyer, M., et al

735 Using the same restraints, the possible conformational docking space of the PB1
736 domains was searched and visualized using DisVis^{44,75,76} with standard parameters.
737 For image creation PyMOLTM (Version 2.1) and UCSF Chimera⁷⁷ were used.

738

739 **Molecular dynamic simulations (MDS) of protein-protein complexes**

740 One refined structure of each group, derived from the cross-link-based docking by
741 HADDOCK incorporating the disorder restraint (2 groups for IAA7^{PB1}·TIR1; 3 groups
742 for IAA12^{PB1}·TIR1), was used as starting structure for MD simulations. The 5 structures
743 were prepared using structure preparation and protonate 3D (pH = 7.5) modules and
744 subsequently minimized with AMBER10 force-field in MOE 2019.0101 (Chemical
745 Computing Group Inc., Montreal, Quebec, Canada).

746 Molecular dynamic simulations were performed with the GROMACS software package
747 (version 4.6.5)⁷⁸. The parameters corresponding to the proteins were generated with
748 AMBER99SB-ILDN force-field⁷⁹, TIP3P explicit solvation model⁸⁰ was used and
749 electro-neutrality was guaranteed with a NaCl concentration of 0.2 mol/L. The protocol
750 employed here to perform MD simulations involves prior energy minimization and
751 position-restrained equilibration, as outlined by Lindahl⁸¹ for lysozyme in water. Once
752 the system was equilibrated, we proceeded to the productive dynamic simulation
753 without position restraint for 20 ns.

754

755 **Effective binding free energy calculations using MM-GBSA**

756 The effective binding free energy (ΔG_{eff}) of the protein-protein complexes formation
757 was calculated using MMPBSA.py from Amber18 package employing the MM-GBSA
758 method⁸². We followed the single trajectory approach, in which the trajectories for the
759 free proteins were extracted from that of the protein-protein complexes. GB^{OBC1} and

Niemeyer, M., et al

760 GB^{OBC2} implicit solvation models were employed⁸². The accumulated mean value of
761 ΔG_{eff} were obtained every 10 ps from the productive MD simulation.

762 Energetically-relevant residues (hot-spots) at the interfaces of TIR1-AUX/IAA PB1
763 complexes were predicted by using the per-residue effective free energy
764 decomposition (prEFED) protocol implemented in MMPBSA.py⁸². Hot-spot residues
765 were defined as those with a side-chain energy contribution (ΔG_{sc}) of ≤ -1.0 kcal/mol.
766 We used Computational Alanine Scanning (CAS)⁸² to further assess per-residue free
767 energy contributions. Alanine single-point mutations were generated on previously
768 identified hot-spots from the prEFED protocol. Both prEFED and CAS protocols were
769 performed from the last 10 ns of the MD simulation.

770
771
772
773
774
775
776
777
778
779
780
781
782
783
784
785
786
787
788
789
790
791
792
793
794
795
796
797
798
799
800
801
802
803
804
805
806
807
808
809
810
811
812
813
814
815
816
817
818
819
820
821
822
823
824

References

1. Chen, B., Retzlaff, M., Roos, T. & Frydman, J. Cellular strategies of protein quality control. *Cold Spring Harb Perspect Biol* **3**, a004374 (2011).
2. Hershko, A. & Ciechanover, A. The ubiquitin system. *Annu Rev Biochem* **67**, 425-79 (1998).
3. Komander, D. & Rape, M. The ubiquitin code. *Annu Rev Biochem* **81**, 203-29 (2012).
4. Oh, E., Akopian, D. & Rape, M. Principles of Ubiquitin-Dependent Signaling. *Annu Rev Cell Dev Biol* **34**, 137-162 (2018).
5. Hua, Z. & Vierstra, R.D. The cullin-RING ubiquitin-protein ligases. *Annu Rev Plant Biol* **62**, 299-334 (2011).
6. Hao, B. et al. Structural basis of the Cks1-dependent recognition of p27(Kip1) by the SCF(Skp2) ubiquitin ligase. *Mol Cell* **20**, 9-19 (2005).
7. Guharoy, M., Bhowmick, P., Sallam, M. & Tompa, P. Tripartite degrons confer diversity and specificity on regulated protein degradation in the ubiquitin-proteasome system. *Nat Commun* **7**, 10239 (2016).
8. Mattioli, F. & Sixma, T.K. Lysine-targeting specificity in ubiquitin and ubiquitin-like modification pathways. *Nat Struct Mol Biol* **21**, 308-16 (2014).
9. Tang, X. et al. Suprafacial orientation of the SCFCdc4 dimer accommodates multiple geometries for substrate ubiquitination. *Cell* **129**, 1165-76 (2007).
10. Guharoy, M., Bhowmick, P. & Tompa, P. Design Principles Involving Protein Disorder Facilitate Specific Substrate Selection and Degradation by the Ubiquitin-Proteasome System. *J Biol Chem* **291**, 6723-31 (2016).
11. Prakash, S., Tian, L., Ratliff, K.S., Lehotzky, R.E. & Matouschek, A. An unstructured initiation site is required for efficient proteasome-mediated degradation. *Nat Struct Mol Biol* **11**, 830-7 (2004).
12. Pietrosevoli, N., Garcia-Martin, J.A., Solano, R. & Pazos, F. Genome-wide analysis of protein disorder in *Arabidopsis thaliana*: implications for plant environmental adaptation. *PLoS One* **8**, e55524 (2013).
13. Pazos, F., Pietrosevoli, N., Garcia-Martin, J.A. & Solano, R. Protein intrinsic disorder in plants. *Front Plant Sci* **4**, 363 (2013).
14. Covarrubias, A.A., Cuevas-Velazquez, C.L., Romero-Perez, P.S., Rendon-Luna, D.F. & Chater, C.C.C. Structural disorder in plant proteins: where plasticity meets sessility. *Cell Mol Life Sci* **74**, 3119-3147 (2017).
15. Staby, L. et al. Eukaryotic transcription factors: paradigms of protein intrinsic disorder. *Biochem J* **474**, 2509-2532 (2017).
16. Chapman, E.J. & Estelle, M. Mechanism of auxin-regulated gene expression in plants. *Annu Rev Genet* **43**, 265-85 (2009).
17. Abel, S., Nguyen, M.D. & Theologis, A. The PS-IAA4/5-like family of early auxin-inducible mRNAs in *Arabidopsis thaliana*. *J Mol Biol* **251**, 533-49 (1995).
18. Worley, C.K. et al. Degradation of Aux/IAA proteins is essential for normal auxin signalling. *Plant J* **21**, 553-62 (2000).
19. Liscum, E. & Reed, J.W. Genetics of Aux/IAA and ARF action in plant growth and development. *Plant Mol Biol* **49**, 387-400 (2002).
20. Tan, X. et al. Mechanism of auxin perception by the TIR1 ubiquitin ligase. *Nature* **446**, 640-5 (2007).
21. Calderón Villalobos, L.I. et al. A combinatorial TIR1/AFB-Aux/IAA co-receptor system for differential sensing of auxin. *Nat Chem Biol* **8**, 477-85 (2012).
22. Gray, W.M., Kepinski, S., Rouse, D., Leyser, O. & Estelle, M. Auxin regulates SCF(TIR1)-dependent degradation of AUX/IAA proteins. *Nature* **414**, 271-6 (2001).
23. Vernoux, T. et al. The auxin signalling network translates dynamic input into robust patterning at the shoot apex. *Mol Syst Biol* **7**, 508 (2011).
24. Tiwari, S.B., Wang, X.J., Hagen, G. & Guilfoyle, T.J. AUX/IAA proteins are active repressors, and their stability and activity are modulated by auxin. *Plant Cell* **13**, 2809-22 (2001).

Niemeyer, M., et al

- 825 25. Flores-Sandoval, E., Eklund, D.M. & Bowman, J.L. A Simple Auxin Transcriptional
826 Response System Regulates Multiple Morphogenetic Processes in the Liverwort
827 *Marchantia polymorpha*. *PLoS Genet* **11**, e1005207 (2015).
- 828 26. Rensing, S.A. et al. The Physcomitrella genome reveals evolutionary insights into the
829 conquest of land by plants. *Science* **319**, 64-9 (2008).
- 830 27. Overvoorde, P.J. et al. Functional genomic analysis of the AUXIN/INDOLE-3-ACETIC
831 ACID gene family members in *Arabidopsis thaliana*. *Plant Cell* **17**, 3282-300 (2005).
- 832 28. Dreher, K.A., Brown, J., Saw, R.E. & Callis, J. The *Arabidopsis* Aux/IAA protein family
833 has diversified in degradation and auxin responsiveness. *Plant Cell* **18**, 699-714
834 (2006).
- 835 29. Moss, B.L. et al. Rate Motifs Tune Auxin/Indole-3-Acetic Acid Degradation Dynamics.
836 *Plant Physiol* **169**, 803-13 (2015).
- 837 30. Ramos, J.A., Zenser, N., Leyser, O. & Callis, J. Rapid degradation of
838 auxin/indoleacetic acid proteins requires conserved amino acids of domain II and is
839 proteasome dependent. *Plant Cell* **13**, 2349-60. (2001).
- 840 31. Winkler, M. et al. Variation in auxin sensing guides AUX/IAA transcriptional repressor
841 ubiquitylation and destruction. *Nat Commun* **8**, 15706 (2017).
- 842 32. Meszaros, B., Erdos, G. & Dosztanyi, Z. IUPred2A: context-dependent prediction of
843 protein disorder as a function of redox state and protein binding. *Nucleic Acids Res* **46**,
844 W329-W337 (2018).
- 845 33. Mutte, S.K. et al. Origin and evolution of the nuclear auxin response system. *Elife*
846 **7**(2018).
- 847 34. Uversky, V.N. Cracking the folding code. Why do some proteins adopt partially folded
848 conformations, whereas other don't? *FEBS Lett* **514**, 181-3 (2002).
- 849 35. Uversky, V.N. A decade and a half of protein intrinsic disorder: biology still waits for
850 physics. *Protein Sci* **22**, 693-724 (2013).
- 851 36. Sigalov, A.B. Structural biology of intrinsically disordered proteins: Revisiting unsolved
852 mysteries. *Biochimie* **125**, 112-8 (2016).
- 853 37. Iacobucci, C. et al. A cross-linking/mass spectrometry workflow based on MS-
854 cleavable cross-linkers and the MeroX software for studying protein structures and
855 protein-protein interactions. *Nat Protoc* **13**, 2864-2889 (2018).
- 856 38. Sinz, A. Divide and conquer: cleavable cross-linkers to study protein conformation and
857 protein-protein interactions. *Anal Bioanal Chem* **409**, 33-44 (2017).
- 858 39. Gotze, M., Iacobucci, C., Ihling, C.H. & Sinz, A. A Simple Cross-Linking/Mass
859 Spectrometry Workflow for Studying System-wide Protein Interactions. *Anal Chem* **91**,
860 10236-10244 (2019).
- 861 40. Korasick, D.A. et al. Molecular basis for AUXIN RESPONSE FACTOR protein
862 interaction and the control of auxin response repression. *Proc Natl Acad Sci U S A*
863 **111**, 5427-32 (2014).
- 864 41. Nanao, M.H. et al. Structural basis for oligomerization of auxin transcriptional
865 regulators. *Nat Commun* **5**, 3617 (2014).
- 866 42. Han, M. et al. Structural basis for the auxin-induced transcriptional regulation by
867 Aux/IAA17. *Proc Natl Acad Sci U S A* **111**, 18613-8 (2014).
- 868 43. Dinesh, D.C. et al. Solution structure of the PsIAA4 oligomerization domain reveals
869 interaction modes for transcription factors in early auxin response. *Proc Natl Acad Sci*
870 *U S A* (2015).
- 871 44. van Zundert, G.C. & Bonvin, A.M. DisVis: quantifying and visualizing accessible
872 interaction space of distance-restrained biomolecular complexes. *Bioinformatics* **31**,
873 3222-4 (2015).
- 874 45. Luo, J., Zhou, J.J. & Zhang, J.Z. Aux/IAA Gene Family in Plants: Molecular Structure,
875 Regulation, and Function. *Int J Mol Sci* **19**(2018).
- 876 46. O'Shea, C. et al. Structures and Short Linear Motif of Disordered Transcription Factor
877 Regions Provide Clues to the Interactome of the Cellular Hub Protein Radical-induced
878 Cell Death1. *J Biol Chem* **292**, 512-527 (2017).

Niemeyer, M., et al

- 879 47. Arai, M., Sugase, K., Dyson, H.J. & Wright, P.E. Conformational propensities of
880 intrinsically disordered proteins influence the mechanism of binding and folding. *Proc*
881 *Natl Acad Sci U S A* **112**, 9614-9 (2015).
- 882 48. Davey, N.E. et al. SLiMPrints: conservation-based discovery of functional motif
883 fingerprints in intrinsically disordered protein regions. *Nucleic Acids Res* **40**, 10628-41
884 (2012).
- 885 49. Zarin, T. et al. Proteome-wide signatures of function in highly diverged intrinsically
886 disordered regions. *Elife* **8**(2019).
- 887 50. Kato, H., Nishihama, R., Weijers, D. & Kohchi, T. Evolution of nuclear auxin signaling:
888 lessons from genetic studies with basal land plants. *J Exp Bot* **69**, 291-301 (2018).
- 889 51. Csizmok, V. et al. An allosteric conduit facilitates dynamic multisite substrate
890 recognition by the SCF(Cdc4) ubiquitin ligase. *Nat Commun* **8**, 13943 (2017).
- 891 52. Keul, N.D. et al. The entropic force generated by intrinsically disordered segments
892 tunes protein function. *Nature* **563**, 584-588 (2018).
- 893 53. Davey, N.E. et al. Attributes of short linear motifs. *Mol Biosyst* **8**, 268-81 (2012).
- 894 54. Abel, S., Oeller, P.W. & Theologis, A. Early auxin-induced genes encode short-lived
895 nuclear proteins. *Proc Natl Acad Sci U S A* **91**, 326-30 (1994).
- 896 55. Bard, J.A.M., Bashore, C., Dong, K.C. & Martin, A. The 26S Proteasome Utilizes a
897 Kinetic Gateway to Prioritize Substrate Degradation. *Cell* **177**, 286-298 e15 (2019).
- 898 56. Fishbain, S. et al. Sequence composition of disordered regions fine-tunes protein half-
899 life. *Nat Struct Mol Biol* **22**, 214-21 (2015).
- 900 57. Fishbain, S., Prakash, S., Herrig, A., Elsasser, S. & Matouschek, A. Rad23 escapes
901 degradation because it lacks a proteasome initiation region. *Nat Commun* **2**, 192
902 (2011).
- 903 58. Ferreon, A.C.M., Ferreon, J.C., Wright, P.E. & Deniz, A.A. Modulation of allostery by
904 protein intrinsic disorder. *Nature* **498**, 390-+ (2013).
- 905 59. Powers, S.K. et al. Nucleo-cytoplasmic Partitioning of ARF Proteins Controls Auxin
906 Responses in Arabidopsis thaliana. *Mol Cell* (2019).
- 907 60. Madeira, F. et al. The EMBL-EBI search and sequence analysis tools APIs in 2019.
908 *Nucleic Acids Res* **47**, W636-W641 (2019).
- 909 61. UniProt, C. UniProt: a worldwide hub of protein knowledge. *Nucleic Acids Res* **47**,
910 D506-D515 (2019).
- 911 62. Letunic, I. & Bork, P. Interactive Tree Of Life (iTOL) v4: recent updates and new
912 developments. *Nucleic Acids Res* **47**, W256-W259 (2019).
- 913 63. Hanson, J., Yang, Y., Paliwal, K. & Zhou, Y. Improving protein disorder prediction by
914 deep bidirectional long short-term memory recurrent neural networks. *Bioinformatics*
915 **33**, 685-692 (2017).
- 916 64. Ishida, T. & Kinoshita, K. PrDOS: prediction of disordered protein regions from amino
917 acid sequence. *Nucleic Acids Res* **35**, W460-4 (2007).
- 918 65. Artimo, P. et al. ExPASy: SIB bioinformatics resource portal. *Nucleic Acids Res* **40**,
919 W597-603 (2012).
- 920 66. Wilkins, M.R. et al. Protein identification and analysis tools in the ExPASy server.
921 *Methods Mol Biol* **112**, 531-52 (1999).
- 922 67. Kyte, J. & Doolittle, R.F. A simple method for displaying the hydropathic character of a
923 protein. *J Mol Biol* **157**, 105-32 (1982).
- 924 68. Uversky, V.N. Use of fast protein size-exclusion liquid chromatography to study the
925 unfolding of proteins which denature through the molten globule. *Biochemistry* **32**,
926 13288-98 (1993).
- 927 69. Hellmuth, A. & Calderón Villalobos, L.I. Radioligand Binding Assays for Determining
928 Dissociation Constants of Phytohormone Receptors. *Methods Mol Biol* **1450**, 23-34
929 (2016).
- 930 70. Webb, B. & Sali, A. Protein Structure Modeling with MODELLER. *Methods Mol Biol*
931 **1654**, 39-54 (2017).

Niemeyer, M., et al

- 932 71. Dominguez, C., Boelens, R. & Bonvin, A.M. HADDOCK: a protein-protein docking
933 approach based on biochemical or biophysical information. *J Am Chem Soc* **125**, 1731-
934 7 (2003).
- 935 72. van Zundert, G.C.P. et al. The HADDOCK2.2 Web Server: User-Friendly Integrative
936 Modeling of Biomolecular Complexes. *J Mol Biol* **428**, 720-725 (2016).
- 937 73. Hamdi, K. et al. Structural disorder and induced folding within two cereal, ABA stress
938 and ripening (ASR) proteins. *Sci Rep* **7**, 15544 (2017).
- 939 74. Rodrigues, J.P. et al. Clustering biomolecular complexes by residue contacts similarity.
940 *Proteins* **80**, 1810-7 (2012).
- 941 75. Nakikj, D. & Mamykina, L. DisVis: Visualizing Discussion Threads in Online Health
942 Communities. *AMIA Annu Symp Proc* **2016**, 944-953 (2016).
- 943 76. van Zundert, G.C. et al. The DisVis and PowerFit Web Servers: Explorative and
944 Integrative Modeling of Biomolecular Complexes. *J Mol Biol* **429**, 399-407 (2017).
- 945 77. Pettersen, E.F. et al. UCSF Chimera--a visualization system for exploratory research
946 and analysis. *J Comput Chem* **25**, 1605-12 (2004).
- 947 78. Pronk, S. et al. GROMACS 4.5: a high-throughput and highly parallel open source
948 molecular simulation toolkit. *Bioinformatics* **29**, 845-54 (2013).
- 949 79. Hornak, V. et al. Comparison of multiple Amber force fields and development of
950 improved protein backbone parameters. *Proteins* **65**, 712-25 (2006).
- 951 80. Jorgensen, W.L., Chandrasekhar, J., Madura, J.D., Impey, R.W. & Klein, M.L.
952 Comparison of Simple Potential Functions for Simulating Liquid Water. *Journal of*
953 *Chemical Physics* **79**, 926-935 (1983).
- 954 81. Lindahl, E. Molecular dynamics simulations. *Methods Mol Biol* **1215**, 3-26 (2015).
- 955 82. Case, D.A.B.-S., I. Y.; Brozell, S. R.; Cerutti, D. S.; T.E. Cheatham, I.; Cruzeiro, V.
956 W. D.; Darden, T. A.; Duke, R. E.; Ghoreishi, D.; Gilson, M. K.; Gohlke, H.; Goetz,
957 A. W.; Greene, D.; Harris, R.; Homeyer, N.; Izadi, S.; Kovalenko, A.; Kurtzman, T.;
958 Lee, T. S.; LeGrand, S.; Li, P.; Lin, C.; Liu, J.; Luchko, T.; Luo, R.; Mermelstein,
959 D. J.; Merz, K. M.; Miao, Y.; Monard, G.; Nguyen, C.; Nguyen, H.; Omelyan, I.;
960 Onufriev, A.; Pan, F.; Qi, R.; Roe, D. R.; Roitberg, A.; Sagui, C.; Schott-Verdugo,
961 S.; Shen, J.; Simmerling, C. L.; Smith, J.; Salomon-Ferrer, R.; Swails, J.; Walker,
962 R. C.; Wang, J.; Wei, H.; Wolf, R. M.; Wu, X.; Xiao, L.; York, D. M.; Kollman, P. A.
963 . AMBER 2018. (University of California, San Francisco, 2018).

964

Niemeyer, M., et al

965 **Acknowledgements**

966 We thank Wolfgang Brandt for initial in silico models of AUX/IAA PB1 domains, and
967 Silvestre Marillonet for the design of constructs for Golden Gate Technology. Thanks
968 to Steffen Abel and Elisabeth Chapman for providing input to the manuscript. This
969 work was supported by the Deutsche Forschungsgemeinschaft (DFG, research
970 project CA716/2-1), and core funding of the Leibniz Institute of Plant Biochemistry
971 (IPB).

Niemeyer, M., et al

972 **Author contributions**

973 M.N. and L.I.A.C.V. prepared the manuscript and designed experiments. M.N.
974 performed biochemical experiments and analyzed the data. M.N., C.I. and C.H.I.
975 carried out XL-MS experiments and data analysis. P.K. and M.N carried out all
976 HADDOCK-based approaches including DisVis, and E.M.C. computational calculation
977 and simulations. M.N., A.H. and V.W. generated Y2H constructs and performed the
978 assays. M.N. performed ubiquitylation experiments, and together with W.H. analyzed
979 mass spectral data of ubiquitylation sites. S.S. and M.Z. carried out ratiometric
980 experiments and analyzed the data. E.M.C., C.I, C.I., P.K., and A.S. provided input to
981 the manuscript. All authors approved the intellectual content.

Niemeyer, M., et al

982 **Competing Interest Statement**

983 The authors declared no competing interests.

Niemeyer, M., et al

984 **Additional Information**

985 Supplementary information is available online. Mass spectrometry proteomics data
986 have been deposited to the ProteomeXchange Consortium via the PRIDE partner
987 repository with the data sets identifiers: PXD015285 (XL-MS) and PXD015392
988 (ubiquitylation site identification data). Correspondence and request for materials
989 should be addressed to L.I.A.C.V.

Niemeyer, M., et al

990 **Figure Legends**

991 **Figure 1| AUX/IAA proteins are intrinsically disordered outside the PB1 domain.**

992 (a) Simplified phylogenetic tree of 29 *Arabidopsis thaliana* AUX/IAAs showing their
993 sequence composition based on IUPred2A prediction for disorder (score classification:
994 disorder: >0.6; intermediate: 0.4-0.6; ordered: <0.4). Outer circles correspond to full
995 length proteins, inner circles represent disorder prediction excluding the PB1 domain.

996 (b) *In silico* prediction maps of disorder along the IAA7 and IAA12 sequence using
997 SPOT, IUPRED1 and PrDos algorithms. AUX/IAA domain structure (Domain I (DI), a
998 linker, a core degron, a degron tail and the Phox/Bem1p (PB1) domain) is displayed.

999 Outer plots represent Kyte-Doolittle hydrophathy (scale from -4 to +4). Dotted line in
1000 PrDos prediction represents a 0.5 threshold. (c) Circular dichroism spectra of IAA7

1001 (orange) and IAA12 (aquamarine) oligomerization and PB1-less deficient variants
1002 (dashed colored lines) show the lack of defined secondary structure elements outside

1003 of the PB1 domain. Reference spectra (gray dotted lines) are depicted. Ellipticity is
1004 calculated as mean residual ellipticity (MRE). (d) IAA7 (orange) and IAA12

1005 (aquamarine) exhibit an extended fold according to Stokes radii determination via size
1006 exclusion chromatography. Theoretical Stokes radii of known folds (gray, labeled

1007 rectangles): intrinsically disordered protein (IDP), pre-molten globule (PMG), molten
1008 globule (MG), natively folded (NF) plus 10% outer limits, and experimental values

1009 (colored box plots) (generated with RStudio, default settings; n = 4-9). IAA7 and IAA12
1010 classify as MG/PMG-like proteins (bm3 variants) with less folded PMG/IDP-like

1011 features outside the PB1 domain (Δ PB1 variants).

1012

Niemeyer, M., et al

1013 **Figure 2| Auxin-dependent TIR1-IAA7 and TIR1-IAA12 interactions rely on the**
1014 **core degron, and a flexible IDR located at a suitable distance between the**
1015 **degron and the PB1 domain. (a)** Y2H interaction matrix (left) for TIR1 with ASK1,
1016 and 16 chimeric proteins built fusing IAA7 and IAA12 segments flanked by
1017 conserved motifs throughout the AUX/IAA family. Yeast diploids containing LexA
1018 DBD-TIR1 and AD-AUX/IAA chimeras were spotted to selective medium with
1019 increasing IAA concentrations, and β -galactosidase reporter expression indicated
1020 auxin-induced TIR1-AUX/IAA interactions. AD-empty vector, negative control.
1021 Domain organization and composition of seamless chimeric IAA7 and IAA12
1022 constructs depicted in boxes (right) with DI (white) (till KR motif), linker (light gray),
1023 core degron (red), degron tail (light pink), and PB1 domain (dark gray). Deleted
1024 domains are indicated (delta (Δ)). **(b-c)** Saturation binding assays using [3 H]IAA to
1025 recombinant ASK1-TIR1-IAA7 (orange) or ASK1-TIR1-IAA12 (aquamarine) ternary
1026 complexes. TIR1-IAA7 complex exhibits a high affinity ($K_d \sim 20$ nM) for auxin,
1027 whereas IAA12-containing co-receptor complexes provide ten-fold lower affinity for
1028 auxin ($K_d \sim 200$ nM). Oligomerization-deficient IAA7bm3 and IAA12bm3 variants, and
1029 chimeric AUX/IAA proteins (IAA_x) in complex with ASK1-TIR1 distinctly affect auxin
1030 bind capabilities of a co-receptor system. Shown are saturation binding curves for
1031 each co-receptor pair as relative [3 H]IAA binding normalized to the highest value of
1032 each curve **(b-c)**. Each point reflects technical triplicates as mean \pm SEM (n=2-3). **(d)**
1033 Comparison of dissociation constants (K_d) obtained in saturation binding
1034 experiments for each ASK1-TIR1-AUX/IAA ternary complex. Shown are mean
1035 values and standard deviation, or maximum and minimum, if applicable.
1036

Niemeyer, M., et al

1037 **Figure 3| Auxin-driven and SCF^{TIR1}-dependent ubiquitylation of IAA7 and IAA12**

1038 **display distinct dynamics. (a)** IVU assays with recombinant GST-IAA7 or GST-
1039 IAA12, E1 (AtUBA1), E2 (AtUBC8), reconstituted SCF^{TIR1} (*AtSKP1*·TIR1, *HsCul1*
1040 and *MmRBX1*), fluorescein-labeled ubiquitin (Ub) and IAA (auxin). IAA7 and IAA12
1041 ubiquitylation is auxin-driven and time-dependent. Basal ubiquitylation (auxin-
1042 independent) of IAA7 starts in less than 30 mins. Ubiquitylation was monitored using
1043 the ubiquitin fluorescent signal (green), and anti-GST/Alexa Fluor 647-conjugated
1044 antibodies for detection of GST-AUX/IAAs (red). ImageQuantTL software was used
1045 for quantification (middle), and generation of merged image (bottom). **(b)** IAA7 and
1046 IAA12 IVU samples were analyzed via LC-MS, and putative ubiquitylation sites
1047 detected by the diGly (or LRGG) Ub remnant after tryptic digest, were mapped
1048 relative to the domain structure. IAA12 Ub sites agglomerate in the region upstream
1049 of the degron (white) and the degron tail (light pink). **(c)** Ubiquitin-conjugation on
1050 chimeric IAA7 and IAA12 proteins in the presence or absence of 1 μ M IAA. IVU
1051 reaction time 1h. Ubiquitin conjugates on chimeric proteins lacking a degron tail or
1052 the PB1 domain are evidently reduced, which is in agreement with the identified
1053 IAA7 and IAA12 Ub sites. (*) Asterisks depict the unmodified AUX/IAAs.

1054

1055 **Figure 4| Structural proteomics using an MS-cleavable cross-linker reveals**

1056 **TIR1·IAA7 and TIR1·IAA12 interaction interfaces. (a)** Workflow for the cross-
1057 linking coupled to mass spectrometry (XL-MS) approach. Recombinant oligomeric-
1058 deficient IAA7 (orange) and IAA12 (aquamarine) proteins, and ASK1·TIR1 (gray and
1059 light pink) were incubated with the DSBU cross-linker, and samples were analyzed
1060 using LC/MS/MS. Cross-linked peptides were identified using the MeroX software.
1061 **(b)** Interaction interfaces (blue) on TIR1 converge in two distinct patches around

Niemeyer, M., et al

1062 residues K217, K226 and T229 (cluster 1) or K485, S503 and K529 (cluster 2)
1063 revealing AUX/IAAs adopt an extended fold when in complex with TIR1. **(c-d)**
1064 Circular depiction of inter-protein (blue) and intra-protein (red) cross-links along IAA7
1065 (orange), IAA12 (aquamarine), TIR1 (light pink) and ASK1 (gray) protein sequence.
1066 Cross-links were identified in at least 2/3 or 3/4 independent experiments (dashed:
1067 2/3 and 3/4; solid lines: 3/3 and 4/4). High number of intra-protein cross-links (red)
1068 within AUX/IAAs show a high degree of flexibility characteristic of intrinsically
1069 disordered regions (IDRs). Specific cross-links within TIR1 are in agreement with the
1070 crystal structure (PDB: 2P1Q). Inter-protein crosslinks (blue) in the ASK1·TIR1·IAA7
1071 complex mainly occurred between the N-terminus of IAA7 and the C-terminus of
1072 TIR1. Regions downstream of the IAA7 and IAA12 degron preferably cross-linked
1073 with a distinct region on TIR1 (K217, K226, T229). Known motifs and protein
1074 domains are displayed. High variability in TIR1·IAA12 cross-links hints toward a
1075 flexible and less-defined interaction interface, which reflect on the low auxin binding
1076 affinity of a TIR1·IAA12 co-receptor complex.

1077

1078 **Figure 5| Cross-linking-based docking substantiates the function of the**
1079 **disordered degron tail positioning the PB1 domain of AUX/IAAs on TIR1.** PB1
1080 domains of IAA7 (light orange) and IAA12 (aquamarine) were docked on the
1081 ASK1·TIR1 (gray, light pink) structure via HADDOCK using cross-linking data as
1082 main constraint. **(a-b)** Including the length of the disordered degron tail of IAA7 (36
1083 aa) or IAA12 (49 aa) as additional restraint, conspicuously reduces the
1084 conformational space, and the number of accessible TIR1·AUX/IAA PB1 complexes
1085 **(c-d)** Visualization of the possible conformational space occupied by the PB1 domain
1086 on the ASK1·TIR1 protein complex without **(c)** or with **(d)** the degron tail length as

Niemeyer, M., et al

1087 distance restraint. The possible interaction space of the IAA12 PB1 domain on TIR1
1088 is much broader than the IAA7 PB1. This is an evidence the conformational space
1089 for the IAA7 PB1 on TIR1 is much more restricted, especially when the degron tail
1090 restraint is built-in. See Supplementary Fig. 12 for best-scoring atomic detailed
1091 models.

1092

1093 **Figure 6| Molecular dynamics (MD) simulations using HADDOCK-based**
1094 **docking models reveal energetic favorable TIR1·AUX/IAA PB1 interacting**
1095 **moieties. (a-b)** Time evolution of instantaneous ΔG_{eff} values over 20 ns identifying
1096 and refining stable TIR1·AUX/IAA PB1 complexes from HADDOCK best scoring
1097 groups. Black lines indicate the accumulated mean value of ΔG_{eff} for each trajectory.
1098 For both complexes, TIR1·IAA7 PB1 (dark and light orange) **(a)**, and TIR1·IAA12
1099 PB1 (blues and green) **(b)**, one stable complex (group 2, light orange (IAA7) or
1100 aquamarine (IAA12)) characterized by a continuous low energetic state was
1101 identified. Dotted vertical line at 10 ns indicates the time point of equilibrium used as
1102 a reference for subsequent analysis. **(c)** Energetically relevant TIR1 residues for
1103 complex stabilization identified by computational alanine scanning (CAS) using MD
1104 trajectories (in **a & b**) from the equilibration time point onwards. **(d)** Stick
1105 representation of CAS identified residues in TIR1 (light pink) localize to the leucine-
1106 rich-repeats 3-6 (LRR3-6) forming a polar patch that allows interaction with the PB1
1107 domain. **(e)** Yeast-two hybrid (Y2H) interaction matrix for TIR1 wild type and TIR1-
1108 mutant versions carrying amino acid exchanges on relevant CAS-identified residues
1109 with ASK1, IAA7 and IAA12 at different auxin concentrations.

1110

Niemeyer, M., et al

1111 **Figure 7| Model for ASK1-TIR1-AUX/IAA complex assembly fine-tuned by IDRs**
1112 **flanking the AUX/IAA core degron.** The F-Box Protein TIR1 of the SCF^{TIR1} E3
1113 ubiquitin ligase recruits AUX/IAA targets for their ubiquitylation and degradation. The
1114 phytohormone auxin and a core degron in AUX/IAAs are essential for AUX/IAA
1115 recognition. Intrinsically disordered regions (IDRs) flanking the degron provide high
1116 flexibility and an extended fold to AUX/IAAs, and influence TIR1-AUX/IAA complex
1117 formation. At least two different routes are possible for dynamic AUX/IAA recruitment
1118 and UPS-mediated degradation: *i)* auxin-triggered association between TIR1 and the
1119 core AUX/IAA degron paves the way for positioning adjacent IDRs, which exposes
1120 ubiquitin acceptor sites for efficient ubiquitylation; *ii)* transient auxin-independent
1121 interactions between IDRs, as well as the PB1 domain in AUX/IAAs and two patches
1122 of residues at opposite sides of TIR1, assist on auxin binding and offer tailored
1123 positioning. The residency time of an AUX/IAA target on TIR1, when assembled in
1124 an SCF-complex, propels processivity of AUX/IAA ubiquitylation, and impinges on
1125 availability of IDRs as initiation sites for degradation by the 26S proteasome.

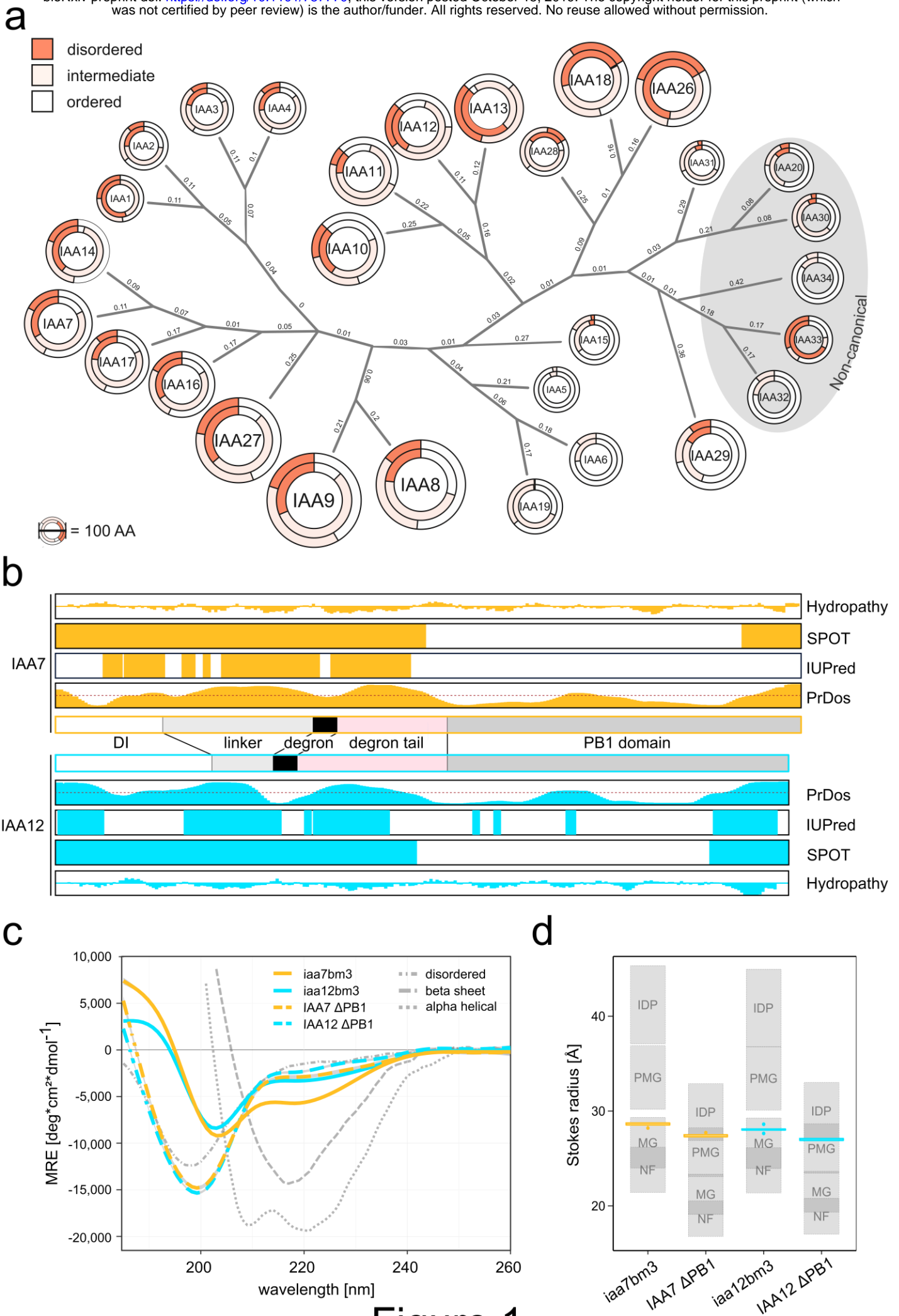
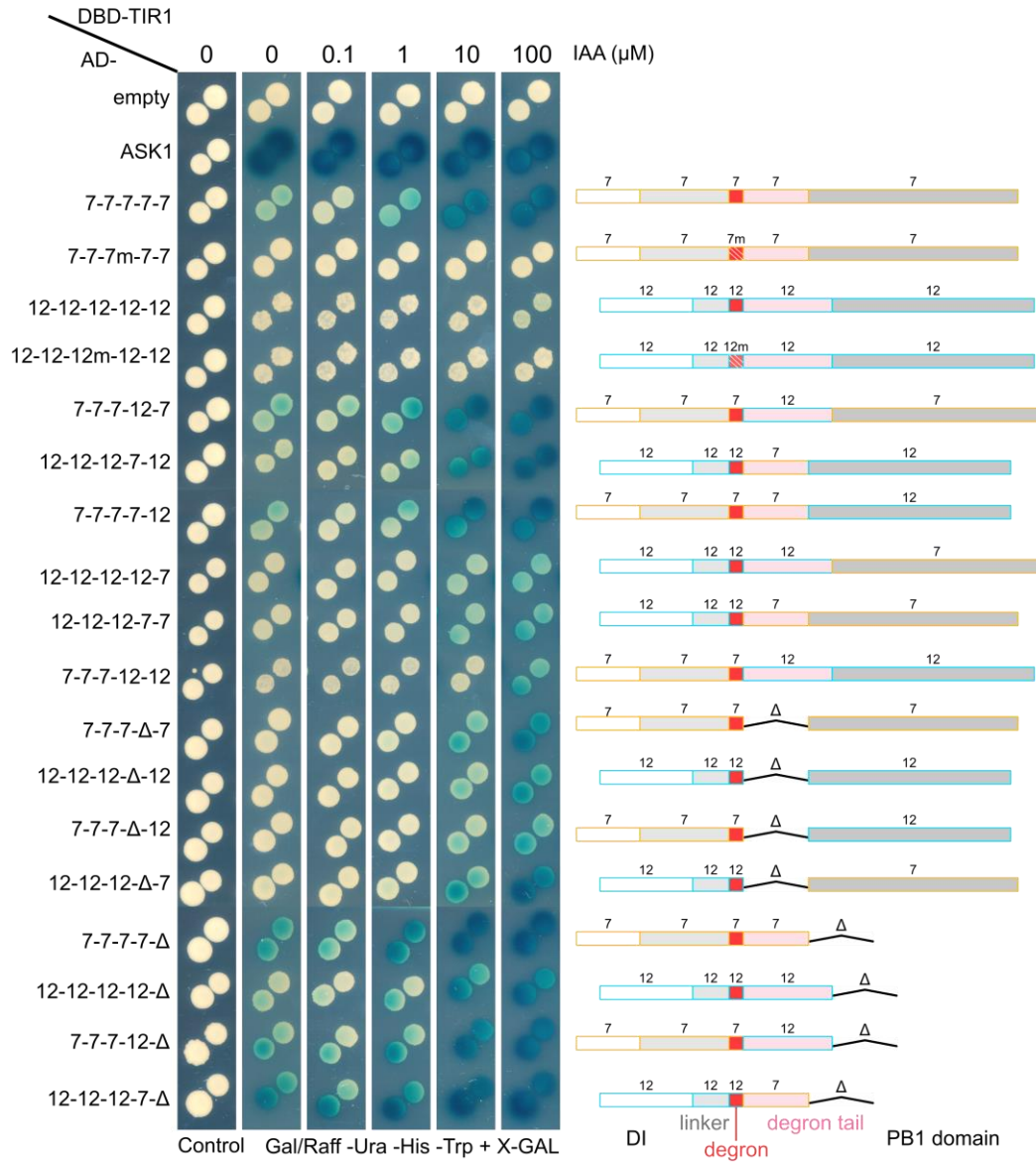
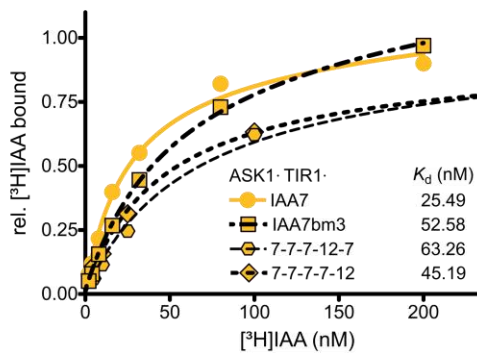


Figure 1

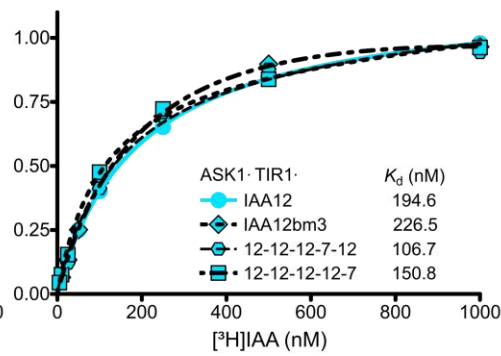
a



b



c



d

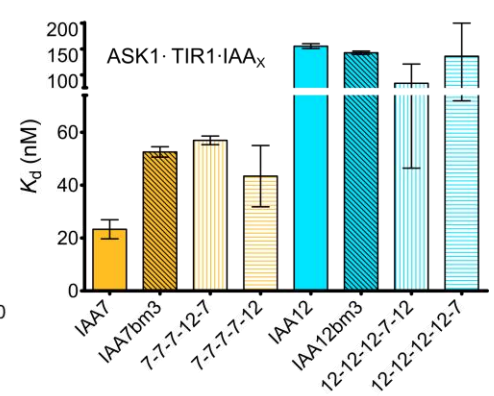
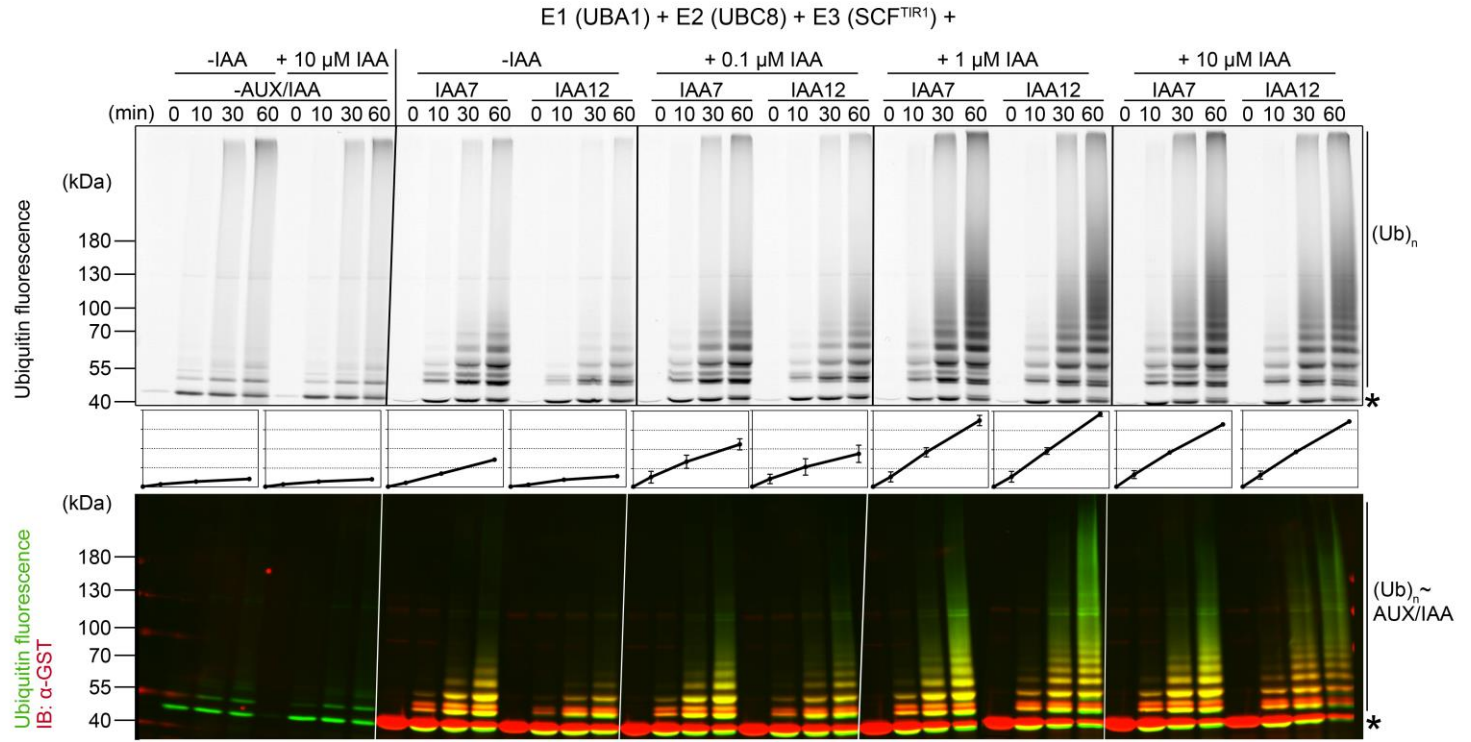
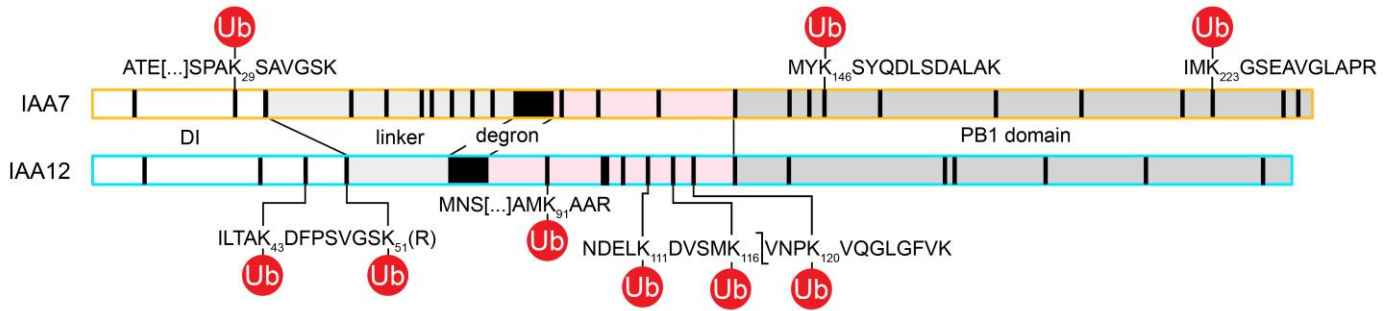


Figure 2

a



b



c

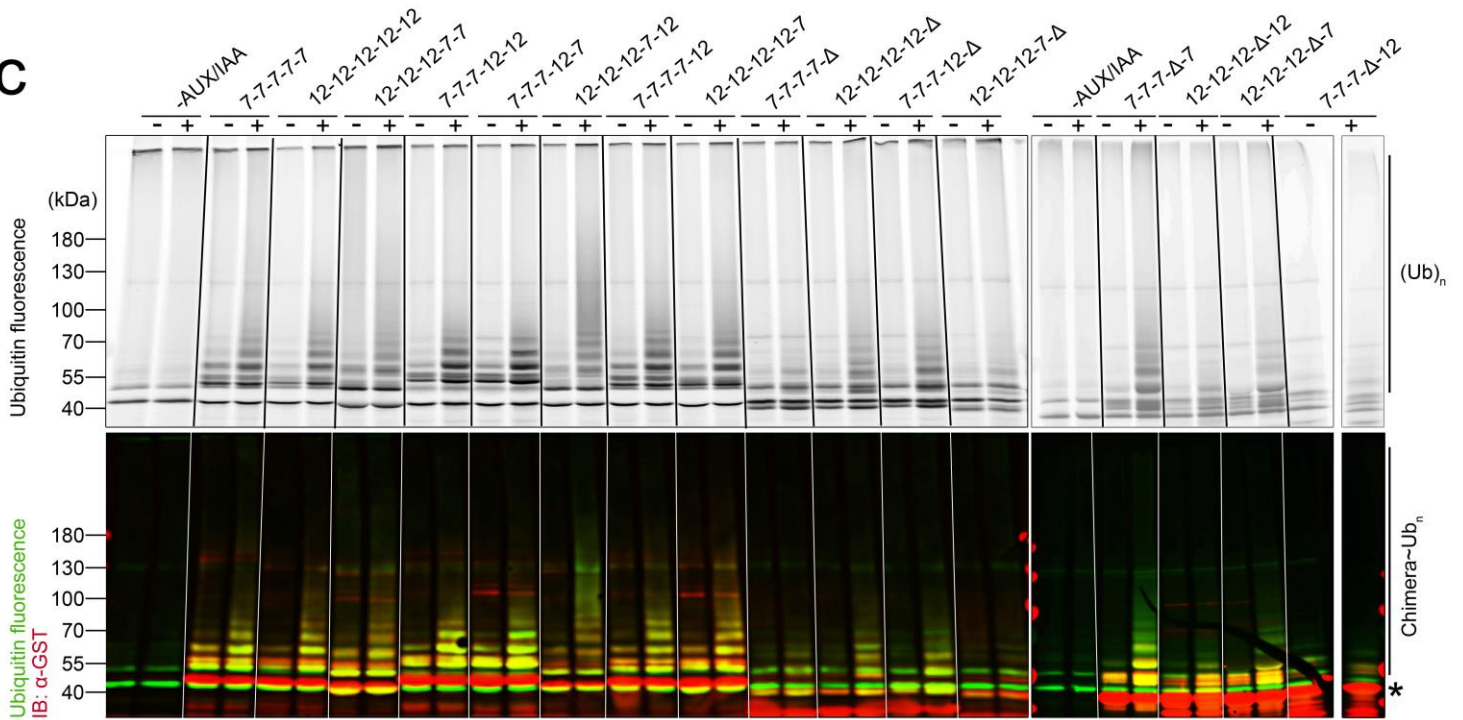


Figure 3

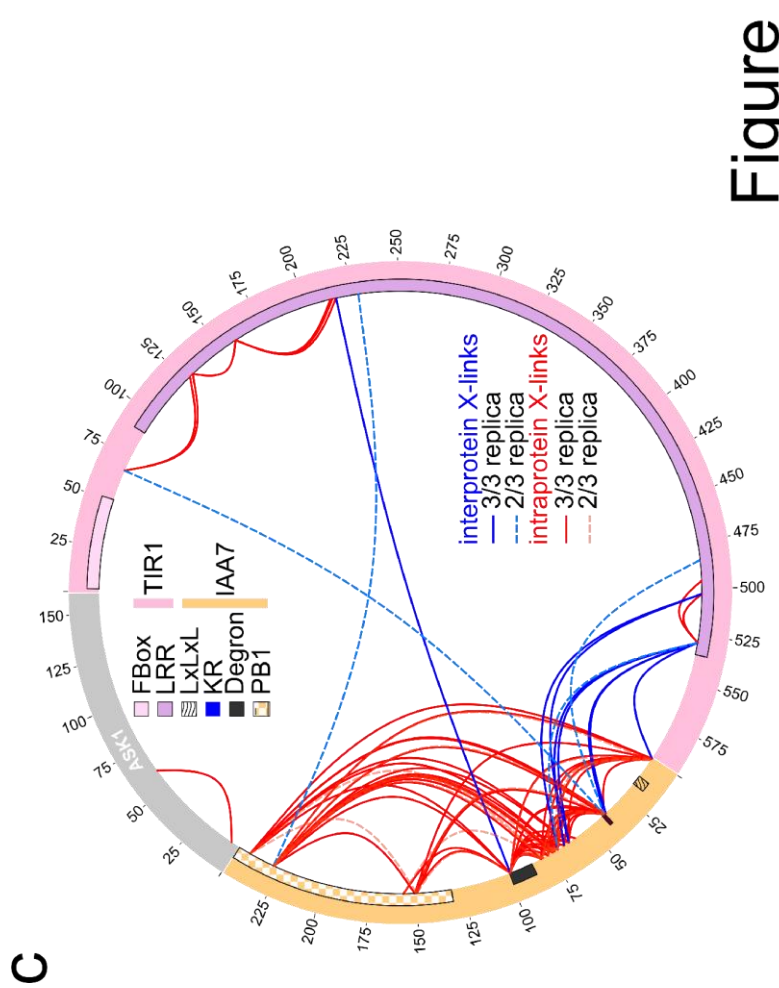
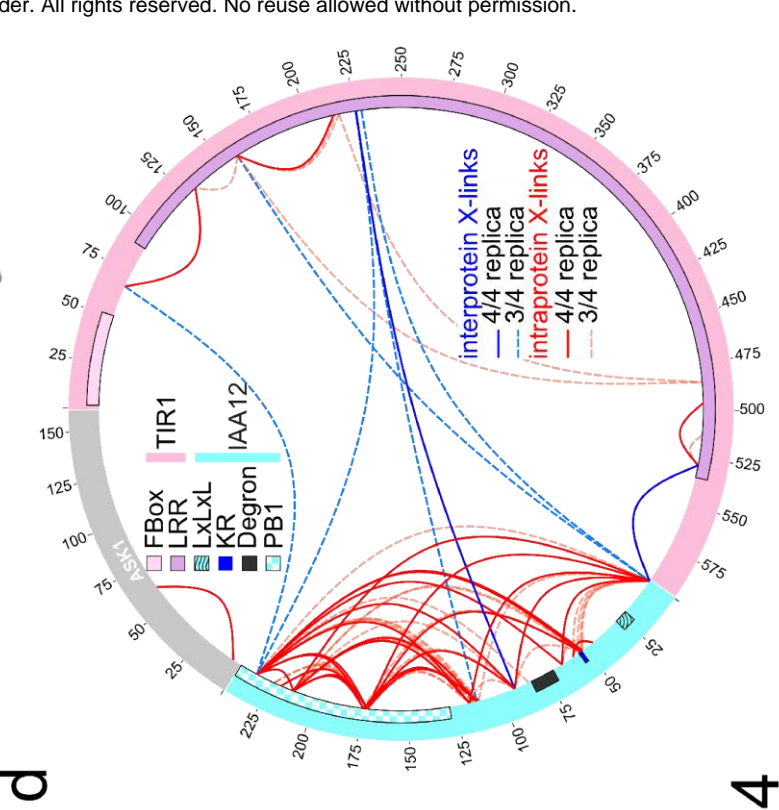
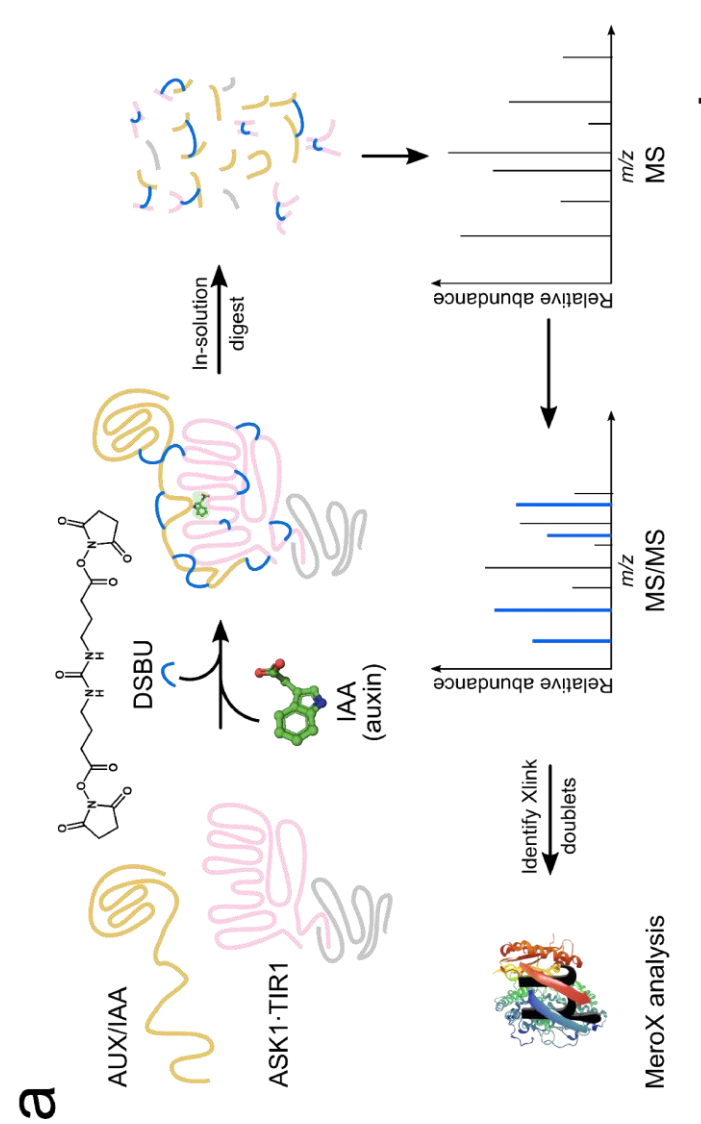
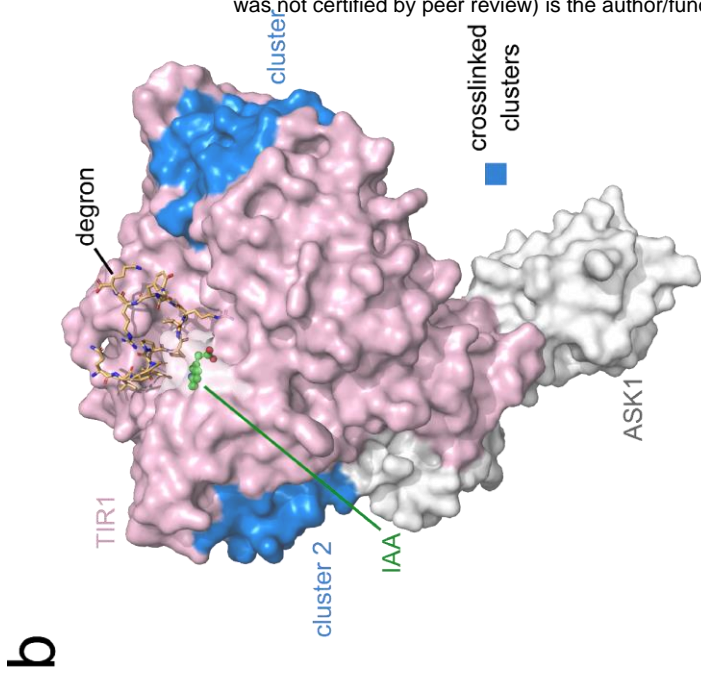


Figure 4

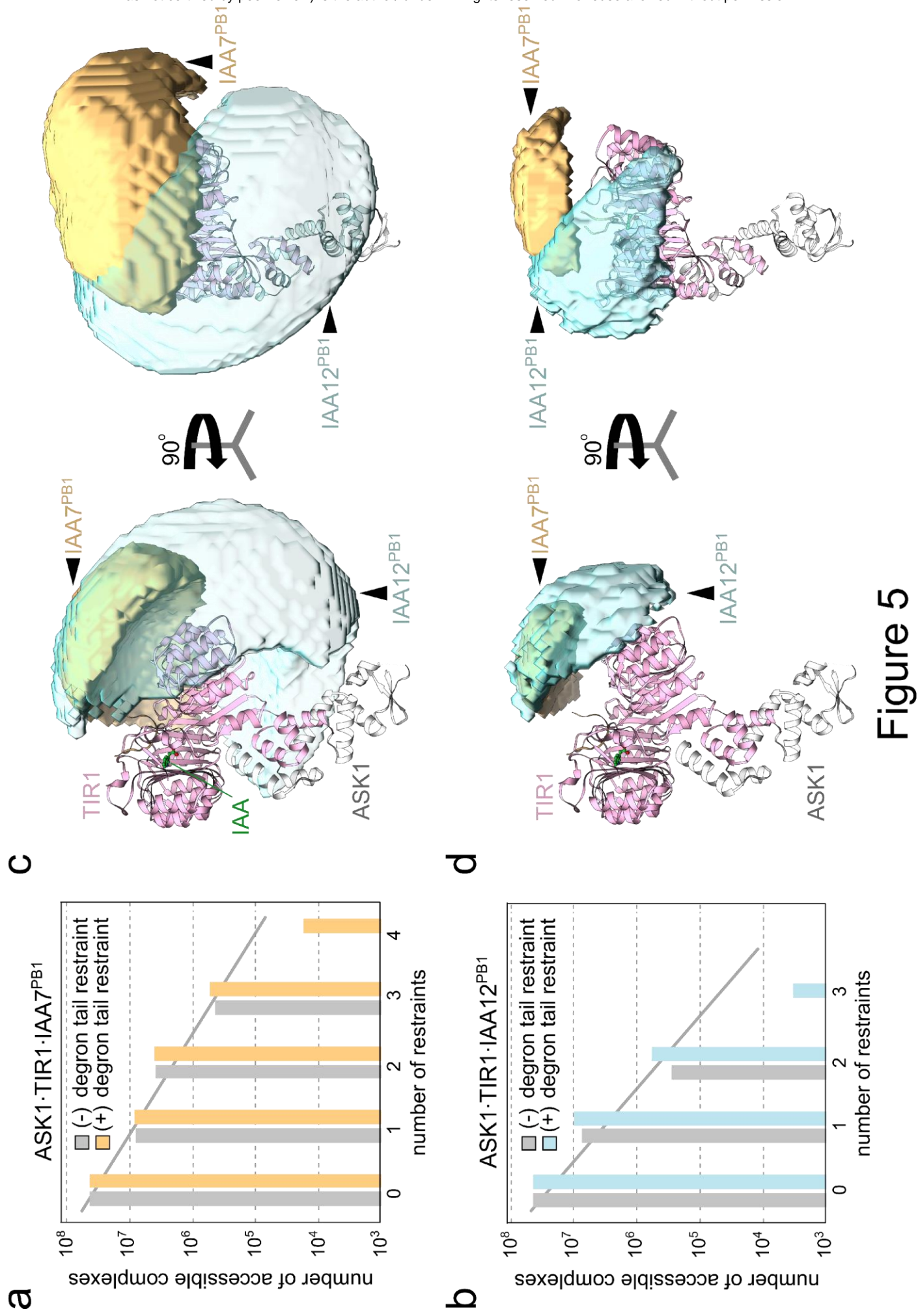


Figure 5

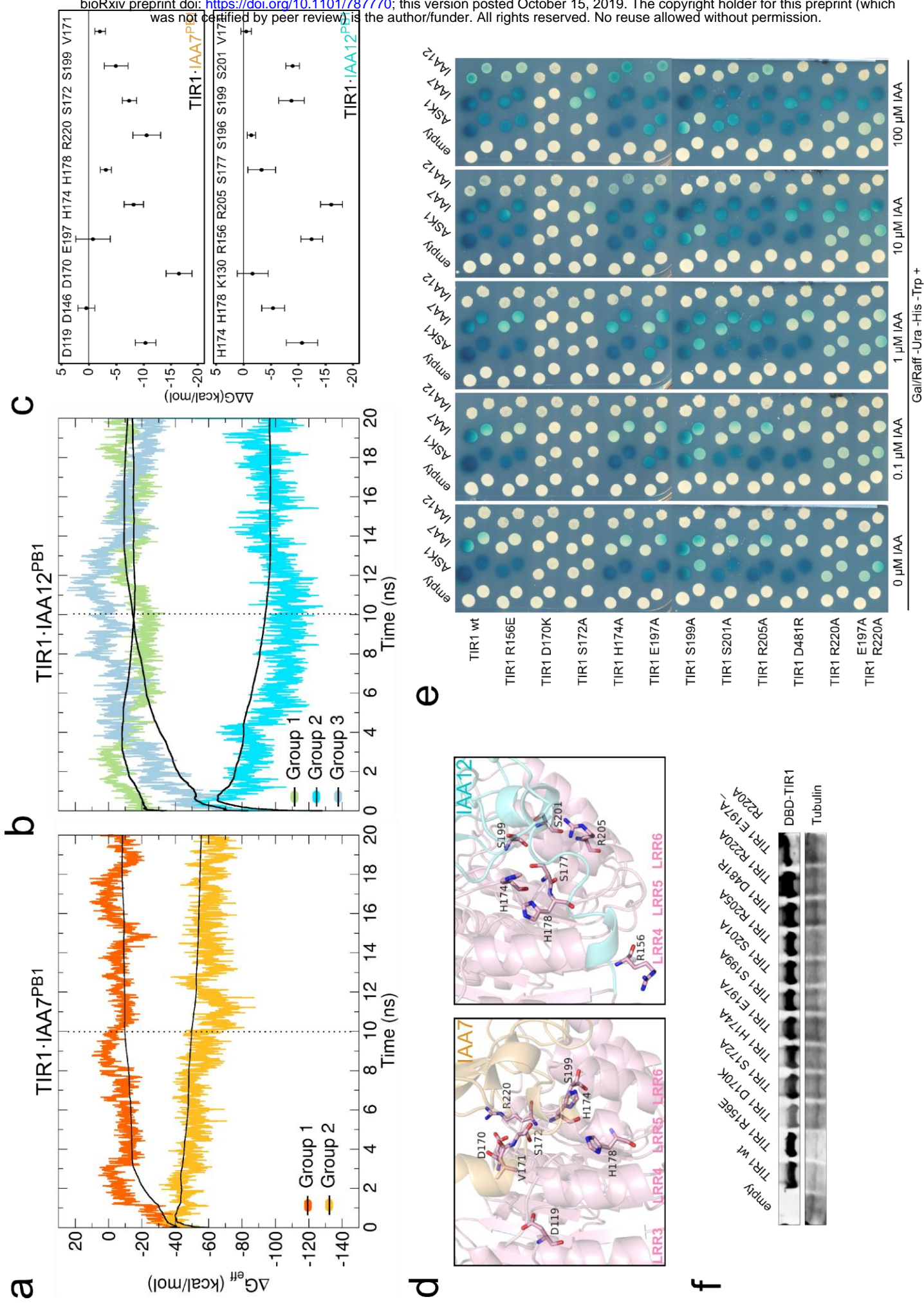
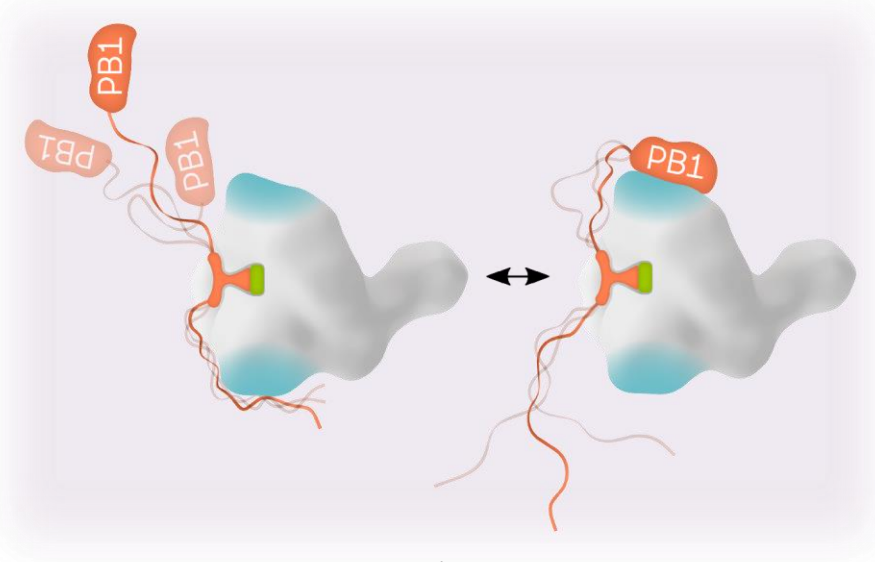
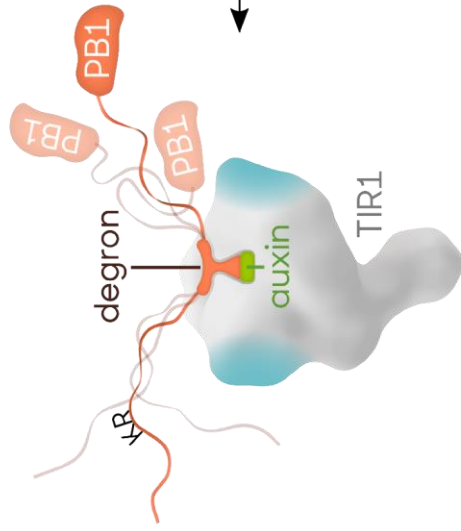
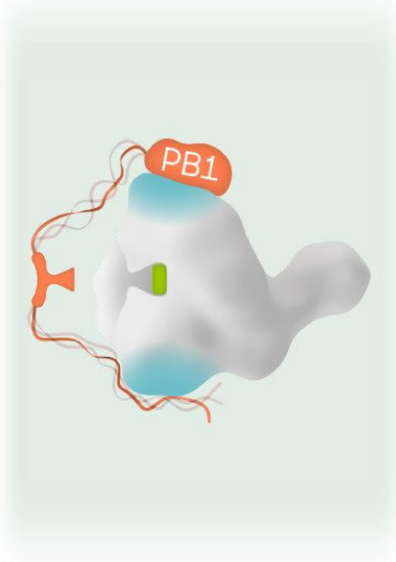


Figure 6

IDR-driven positioning



Guided auxin binding



Auxin-triggered binding

Allosteric P-P interactions
Ubiquitin-mediated proteasomal degradation

Figure 7